

# A quantum phase-space equivalence leads to hidden causal loops in a model for measurement consistent with macroscopic realism

M. D. Reid and P. D. Drummond

*Centre for Quantum Science and Technology Theory,  
Swinburne University of Technology, Melbourne 3122, Australia*

While Bell nonlocality can be explained through mechanisms such as retrocausality and superluminal disturbance, these explanations are not generally thought to be equivalent to quantum mechanics. If such mechanisms exist, it is unclear why such effects do not manifest macroscopically. It is also unclear whether macroscopic realism, arguably a requirement for macroscopic causality, holds. In this paper, we show how unobservable causal loops arise from quantum mechanics, and can explain quantum measurement consistently with macroscopic realism. We analyze a measurement  $\hat{x}$  on a system prepared in a superposition of eigenstates  $|x_j\rangle$  where the measurement is modeled by amplification. Deriving path-integral theorems, we prove an equivalence between the positive phase-space distribution  $Q(x, p, t)$  which represents the quantum state, and simultaneous backward- and forward-propagating stochastic trajectories for amplitudes  $x$  and  $p$ . The sampling for the amplified variable  $x$  is specified by a future boundary condition determined by the measurement setting, the backward and forward trajectories being linked at the initial-time boundary to form a loop. We confirm that the joint densities for  $x(t)$  and  $p(t)$  yield  $Q(x, p, t)$ , thus demonstrating causal consistency and Born's rule. A feature is "hidden" vacuum noise associated with an eigenstate. Unlike the eigenvalue  $x_j$ , this noise is not amplified, the fluctuations originating from future boundary conditions. For macroscopic superpositions of  $|x_j\rangle$ , we show consistency with macroscopic realism: the outcome for  $\hat{x}$  can be considered a real property at the time  $t_0$  prior to measurement (independent of future events). We deduce a hybrid causal structure involving causal relations for amplified variables, along with hidden causal loops for unamplified quantities, demonstrating that causal loops do not imply (observable) retrocausality. Further, we evaluate  $Q_j(x, p, 0)$  for the trajectories conditioned on the outcome  $x_j$ . The "state" defined by this function cannot correspond to a quantum state, the uncertainties for  $\hat{x}$  and  $\hat{p}$  being too small. However,  $Q_j(x, p, 0)$  approaches that of  $|x_j\rangle$  for a macroscopic superposition. Our results motivate analyses of Schrödinger's paradox and the measurement problem, and provide a framework for study of Einstein-Podolsky-Rosen and Bell correlations.

## I. INTRODUCTION

Following from Bohr [1] who considered delayed-choice experiments [2], Wheeler speculated that retrocausality due to future boundary conditions may explain quantum paradoxes [3, 4]. Retrocausal dynamics was studied in classical physics even earlier [5–7]. Bell and subsequent experiments proved that all local causal theories could be falsified, based on quantum predictions allowing a violation of Bell inequalities [8–10]. Violations of Bell inequalities can arise from classical fields, however, using retrocausal, i.e. advanced, solutions from absorber theory [11–14]. Bell's work motivated the question of whether superluminal disturbances were possible, leading to no-signaling theorems [15]. These studies inspired many analyses of causality in quantum physics [2, 16–46].

Studies of causal structure are closely related to studies of realism in quantum mechanics. If retrocausal or superluminal mechanisms exist, why are such mechanisms not apparent at a macroscopic level? Classical causal models assume real properties that describe the system at a given time; non-retrocausal models imply these cannot be changed by future events. Since causality is observed macroscopically, we would expect that macroscopic realism holds. Yet, for systems in a macroscopic superposition state, Schrödinger pointed out this suggests quantum mechanics to be an incomplete descrip-

tion [47]. These questions are linked to the measurement problem. For a system in a superposition of eigenstates of the measurement operator, the state after the measurement 'collapses' to just one of these states. Is there a more complete description for how this occurs? Different resolutions have been proposed (e.g. [48–53]). One can also suggest a purely statistical interpretation, although this leads to Born's question of "what is the reality which our theory has been invented to describe?" [54], and similar objections by Bell [55].

There has been recent interest in the causal structure of quantum correlations [56–77]. Causal modelling has given insight into quantum networks [78], paradoxes [34, 45, 79, 80] and quantum information and computation [81–84]. Bell violations can be explained using classical causal models, but this entails solutions based on, for instance, superluminal causal influences [48, 85–87], retrocausality [11, 24, 42], or superdeterminism [88]. A criticism is that these mechanisms require a fine-tuning of causal parameters to explain an observed statistical independence of variables [58–60] – an exception to this being retrocausal effects that induce cyclic causal loops [58, 78, 89]. It has been proposed that hidden causal loops explain nonlocality and quantum speed-up [90–92]. Moreover, recent work reveals that cyclic loops are not excluded by no-signalling theorems [89]. Regardless, the mystery remains that retrocausality is not observed at a macroscopic level. Quantum causal models have been de-

veloped to address these problems [61–67]. It remains not clear however whether one can present a unified framework combining causality and realism, and at what level (from microscopic to macroscopic) causal concepts hold.

In this paper, we analyze quantum measurement using a quantum field model motivated by phase-space dynamics based on the  $Q$  function [53, 93, 94]. A measurement of  $\hat{x}$  of a single-mode field is modelled by parametric amplification, which amplifies  $\hat{x}$ . We derive a path-integral theorem linking the evolution of the quantum phase-space distribution function  $Q(x, p, t)$  to the stochastic dynamics of real *amplitudes*  $x$  and  $p$  involving *both forward- and backward-propagating* trajectories in time. The model provides an explanation of quantum measurement based on dynamics due to future boundary conditions determined by the measurement setting—there is no sudden “collapse” of the wave-function. The  $Q$ -based model allows for cyclic causation, and is therefore immune to the fine-tuning arguments in which directed acyclic graph theory excludes retrocausality as a solution [58–60].

The forward-backward stochastic behavior is derived from quantum mechanics, emerging as a result of microscopic noise sources generated by interactions. This distinguishes the theory from previous analyses involving toy models [24, 95], and allows a analysis of causal structure and models of realism in terms of the dynamics of the amplitudes. The analysis reveals causal loops for unobservable (hidden) variables, yet gives consistency with macroscopic realism, hence laying the foundation for macroscopic causality.

In summary, it is shown in this paper that the following results hold for the measurement model:

1. The dynamics is modeled by a set of stochastic trajectories  $x(t)$  that have boundaries in the future, and  $p(t)$  with boundaries in the past.
2. The density of the trajectories  $x(t_f)$  at the time  $t_f \rightarrow \infty$  is proportional to the probability for an outcome  $x$  of  $\hat{x}$ , giving agreement with Born’s rule.
3. The  $Q$  function and hence the quantum moments are equivalently evaluated by averaging over the trajectories for  $x(t)$  and  $p(t)$ . This proves a causal consistency that the future boundary condition does not change the current quantum state, given uniquely by  $Q(x, p, t)$ .
4. A causal cyclic structure is identified as arising from the boundary conditions, linking the  $x(t)$  and  $p(t)$  trajectories. This structure involves variables that are not measurable.
5. The linked trajectories for  $x(t)$  and  $p(t)$  define a calculable distribution  $Q_j$  for each possible outcome given by an eigenvalue  $\lambda_j$ . This distribution cannot correspond to a quantum state  $|\psi_j\rangle$ , except in certain cases.

6. From (4), we demonstrate consistency with macroscopic realism, as defined by Leggett and Garg [96]. The solutions show how macroscopic realism emerges, as the system is amplified. The hidden causal non-acyclic structure does not imply retro-causality for the amplified variables.

The layout of the paper is as follows. We give an summary of the results in Section II. In Section III, we explain the measurement model and in Section IV, we give details of the stochastic method and path-integral Theorem. In Section V, we solve the equations modeling a measurement  $\hat{x}$  on the system prepared in a superposition of eigenstates of  $\hat{x}$ , using the amplification model  $H_A$ . The results are generalized to superpositions of coherent states, and to the measurement of the complementary observable  $\hat{p}$ . The realization of Born’s rule is explained. The coupling of the  $x$  and  $p$  trajectories is calculated in Section VI. We give details of the causal model in Section VII. The structure allows certain models of realism (including objective-field realism and weak realism) to be considered, which are discussed in Section VIII. In particular, the results are entirely consistent with macroscopic realism, as explained in Section VIII. The Schrödinger-cat paradox and measurement problem is also discussed, in Section IX. A conclusion is given in Section X.

## II. SUMMARY OF PAPER

We consider a single-mode field, for which  $Q$  is the Husimi  $Q$  function  $Q(x, p)$ , and solve for the trajectories of  $x$  and  $p$ , for a measurement process. The measurement of a field quadrature  $\hat{x}$  is modeled by a parametric amplification interaction  $H_A$  which amplifies the  $\hat{x}$  observable. The amplified variable  $x$  corresponds to a backward propagating trajectory, and is sampled according to a future boundary condition determined by the measurement setting. The variable  $p$  is attenuated and corresponds to a forward-propagating trajectory. A distinctive feature of the  $Q$  model is the existence of *hidden vacuum noise*  $\xi(t)$ , of order  $\hbar$ , associated with eigenstates  $|x_j\rangle$  of  $\hat{x}$ .

In order to analyze the measurement problem, we consider a system initially in a superposition  $|\psi\rangle = \sum_j c_j |x_j\rangle$  of eigenstates  $|x_j\rangle$  of  $\hat{x}$  (Figure 1). We solve for the dynamics under  $H_A = \frac{i\hbar g}{2} [\hat{a}^{\dagger 2} - \hat{a}^2]$  for  $g > 0$ , which gives an explicit physical model of a simple meter,  $a$ ,  $\hat{a}^\dagger$  being the boson operators for the field. In the simulations, the trajectories for the *amplified*  $x$  converge to the measurement outcome  $x_j$ . This occurs because while the eigenvalue  $x_j$  is amplified by a factor  $G = e^{gt}$ , the hidden vacuum noise  $\xi(t)$  is not. After correcting for the amplification due to the measurement, we find that the density of amplitudes is  $P_B(x_j) = |\langle x_j | \psi \rangle|^2$ , corresponding to Born’s rule. The noise values  $\xi_x(t)$  for the trajectory of  $x$  are determined retrocausally, from future boundary conditions. The original value of  $x$  (including the noise) at  $t = 0$  is not amplified in its entirety, and hence is not

precisely measurable. We also treat momentum measurements, showing the expected complementary behavior.

The stochastic approach leads to new results. We prove that the  $x$  and  $p$  trajectories are connected according to an initial-time boundary value, in a way not previously calculated from quantum mechanics. A conditional distribution  $P_Q(p|x)$  defined at the initial time  $t = 0$  (just prior to the measurement) dictates the nature of the coupling. For a system prepared in a superposition of eigenstates  $|x_j\rangle$  at time  $t = 0$ , the  $x$  and  $p$  trajectories are linked: a backward propagating trajectory for  $x$  couples to a given set of  $p$  trajectories. This forms part of a causal loop (Figure 1), which signifies a quantum superposition. If prepared in a mixture of eigenstates  $|x_j\rangle$ , the  $x$  and  $p$  trajectories are uncorrelated, and no loop is formed.

The joint probability density for the  $x$  and  $p$  trajectories can be computed, for any stage of the measurement dynamics, and confirmed by statistical comparisons to correspond to the correct quantum  $Q$  function,  $Q(x, p, t)$ . The probability density  $Q$  obtained from the forward (causal) and backward (retrocausal) trajectories depends on the time  $t$  from the initial preparation time  $t = 0$ , and is hence causal, being independent of the time  $t_f$  of the future boundary condition. Thus ‘causal consistency’ arises naturally, and follows because the vacuum noise  $\xi(t)$  is not amplified. Similar results are obtained in absorber theory [6, 7, 14] and analyses of closed timelike curves [97].

The equivalence for  $Q$  motivates an interpretation—objective field realism (OFR)—that there is an underlying reality (in the sense of Born [54]) in which amplitudes  $x$  and  $p$  correspond to a ‘state’ at time  $t$  for the system, with a probability  $Q(x, p, t)$ . There is “objectivity” in the sense of Wheeler-Feynman’s absorber theory based on classical electrodynamics, where fields are assumed to exist independently of any observer. The amplitudes  $x$  and  $p$  however are not directly measurable.

An interesting question is whether there can be any consistency with the notion of realism—that the system is in a ‘state’ with definite outcome,  $x_j$ , prior to measurement. We evaluate the connected trajectories for  $x$  and  $p$ , *conditioned* on a given measurement outcome  $x_j$ . This defines a unique distribution  $Q_j(x, p, 0)$  at the time  $t = 0$ , which we demonstrate cannot correspond to a *quantum* state—the outcomes for  $\hat{x}$  and  $\hat{p}$  would be more precise than permitted by the uncertainty principle. We solve for the superposition

$$|\psi_{sup}\rangle = (|x_1\rangle + |x_2\rangle)/\sqrt{2}, \quad (2.1)$$

finding that the  $Q_j(x, p, 0)$  approaches that of the eigenstate  $|x_j\rangle$  as the separation  $\Delta = |x_1 - x_2|$  becomes larger i.e. for macroscopic superpositions. Perhaps surprisingly, the distribution shows fringes in  $p$  for *each*  $x_j$ , these becoming finer with increased  $\Delta$ . The solutions illustrate the tension between the notion of realism (where the system is in a specified state prior to measurement) and the

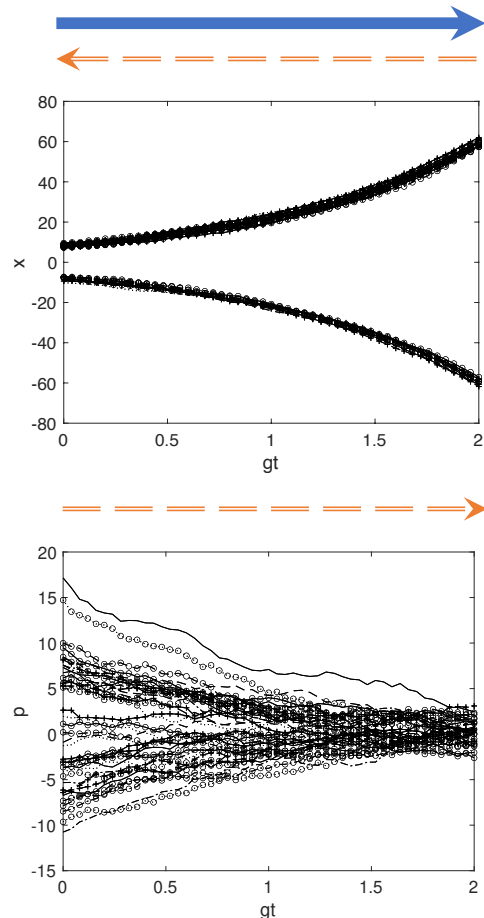


Figure 1. Simulations for the measurement of  $\hat{x}$  on a system prepared in a macroscopic superposition  $|\psi_{sup}\rangle$  (2.1) with  $x_1 = -x_2 = 8$ . The top figure shows trajectories for  $x$  as the system evolves for a time  $t$  under  $H_A$  which amplifies  $\hat{x}$ . The stochastic trajectories propagate backwards from the future boundary at  $gt = 2$ , from either  $Gx_1$  or  $-Gx_1$  ( $G = e^{gt}$ ), but subject to a future noise input  $\xi_x(t)$  with variance at the vacuum level,  $\sigma_x^2 = 1$ . The noise is not amplified or attenuated. The inferred outcome for  $x$  after amplification is  $x(t)/G$ , giving either  $x_1$  or  $-x_1$  with an error that becomes smaller with  $G$ . For the macroscopic superposition, the amplitudes  $x(0)$  at  $t = 0$  indicate the final inferred outcome to be  $x_1$  or  $-x_1$ . This gives a macroscopic causal relation (solid blue line). The actual individual trajectories stemming from each final value are retrocausal however, being subject to the noise  $\xi_x(t)$  (red dashed line). The lower figure shows the forward-propagating trajectories for the complementary variable  $p$ . Here, the values are attenuated to the vacuum noise level,  $\sigma_p^2 = 1$ . A conditional relation at the boundary  $t = 0$  connects the  $x$  and  $p$  trajectories creating a hidden loop (red dashed line). The  $|\psi_{sup}\rangle$  is approximated by (3.16) with  $r = 2$ .

completeness of quantum mechanics, as pointed out by Schrödinger in his famous cat paradox [47].

There is however a provable consistency with macroscopic realism. We show that the density of trajectory values  $x(t)$  after amplification corresponds to the prob-

ability of observation of the result  $x(t)/G$  where  $G$  is the amplification factor, giving agreement with Born's rule. For the macroscopic superposition, where  $\Delta \rightarrow \infty$ , macroscopic realism posits that the system has a *pre-determined value* for the outcome of  $\hat{x}$  (i.e.  $x_1$  or  $x_2$ ). The solutions validate macroscopic realism, the predetermined value being  $x(t)/G$ . The causal structure is determined from the trajectories of  $x$ . There is a hybrid structure: given as causal macroscopically, but retrocausal microscopically (Figure 1). The  $p$  trajectories are causal but microscopic. The causal structure also supports a model of realism, weak realism (wR), in which the measurement setting plays an important role. The Schrödinger-cat paradox [47] is analyzed using  $|\psi_{sup}\rangle$  and the superposition  $|cat\rangle$  of two coherent states. In the model, the paradox arises not because of a failure of macroscopic realism, but because the function  $Q_j(x, p, 0)$  inferred at  $t = 0$ , postselected on the outcome  $x_j$ , cannot be described as a quantum state.

Do the forward-backward solutions for the measurement dynamics give insight into the measurement problem? Since for any superposition  $|\psi_{sup}\rangle$ , the system evolves into a macroscopic superposition under the amplification  $H_A$ , and since  $Q_j(x, p, 0)$  approaches the  $Q$  function of the eigenstate  $|x_j\rangle$ , as  $\Delta \rightarrow \infty$ , this solutions model the “collapse” of the wave function as arising from amplification. However, as  $H_A$  is reversible, this does not give a complete picture. A full treatment would model the coupling to a different system that forms a final meter, giving a read-out to an observer.

### III. MEASUREMENT MODEL

In this paper, the system dynamics is described by a unified stochastic model motivated by the  $Q$  function [98]. The examples of this paper use bosonic fields. The approach requires the measurement process to be included in the dynamics. For this purpose, we use a model of a common measuring device that produces macroscopic outputs, namely the parametric amplifier [99]. These are not fundamental physical restrictions. Fermionic  $Q$ -functions exist [100, 101], and have similar dynamical properties and equations. We expect other models of meters to have analogous behavior.

The measurement problem addresses a quantum state expressed as a linear combination of eigenstates  $|x_j\rangle$  of  $\hat{x}$

$$|\psi_{sup}\rangle = \sum_j c_j |x_j\rangle \quad (3.1)$$

where  $c_j$  are probability amplitudes. The Copenhagen measurement postulate asserts that for such a state, the set of possible outcomes of the measurement  $\hat{x}$  is the set  $\{x_j\}$  of eigenvalues of  $\hat{x}$ . The probability of a given outcome  $x_j$  is  $P_j = |c_j|^2$ . After the measurement, the system “collapses” into the eigenstate  $|x_j\rangle$  associated with that outcome  $x_j$ . The measurement problem is to understand the transition from the state  $|\psi\rangle$  to the final state  $|x_j\rangle$ .

We will investigate the interpretation of the measurement postulate for this stochastic model [53]. In the approach of this paper, the quantum state is epistemological, and no physical collapse occurs.

#### A. Measurement model: parametric amplification

First, restricting our analysis to a single mode for clarity, we define the complementary quadrature phase amplitude  $\hat{x}$  and  $\hat{p}$  observables

$$\begin{aligned} \hat{x} &= \hat{a} + \hat{a}^\dagger \\ \hat{p} &= (\hat{a} - \hat{a}^\dagger)/i \end{aligned} \quad (3.2)$$

where  $\hat{a}$  is the boson destruction operator [102]. This implies  $\Delta\hat{x}\Delta\hat{p} \geq 1$ .

We analyze the simplest measurement procedure that can take place – that of direct amplification to a macroscopic signal. We take a simple model of measurement using a parametric amplifier in a rotating frame, as in current low noise photonic or superconducting experimental measurements. To measure  $\hat{x}$ , the system prepared in  $|\psi_{sup}\rangle$  is amplified according to a unitary interaction [99]

$$H_A = \frac{i\hbar g}{2} [\hat{a}^{\dagger 2} - \hat{a}^2] \quad (3.3)$$

where  $g > 0$  is real. The system evolves according to  $H_A$  for a time  $t_f$ , to give the final measurement output. The measurement is completed simply by the fields being amplified to become macroscopic, and hence detectable to macroscopic devices or observers. No special “collapse” is required, only normal physical processes. For  $g > 0$ , it is known that the dynamics of  $H_A$  gives solutions that amplify the “position”  $\hat{x}$  but attenuate the orthogonal “momentum” quadrature  $\hat{p} = (\hat{a} - \hat{a}^\dagger)/2i$ . This is clear from the standard operator Heisenberg equations which give the solutions

$$\begin{aligned} \hat{x}(t) &= \hat{x}(0) e^{gt} \\ \hat{p}(t) &= \hat{p}(0) e^{-gt}. \end{aligned} \quad (3.4)$$

The Hamiltonian  $H_A$  is equivalent to the Hamiltonian required to induce squeezing in  $\hat{p}$ . The solutions give for the means  $\bar{x}$  and variances

$$\begin{aligned} \langle(\Delta\hat{x})^2\rangle &= \langle\hat{x}^2(t) - \bar{x}^2\rangle = e^{2gt} \\ \langle(\Delta\hat{p})^2\rangle &= \langle\hat{p}^2(t) - \bar{p}^2\rangle = e^{-2gt} \\ \bar{x} &= \langle\hat{x}\rangle = \langle\hat{x}(0)\rangle e^{gt} \\ \bar{p} &= \langle\hat{p}\rangle = \langle\hat{p}(0)\rangle e^{gt}. \end{aligned} \quad (3.5)$$

#### B. Single-mode $Q$ function

To solve for single-mode evolution, we use the  $Q$  function [98]

$$Q(x, p) = \frac{1}{\pi} |\langle\alpha|\psi\rangle|^2, \quad (3.6)$$

defined for a quantum state  $|\psi\rangle$  with respect to the nonorthogonal basis of coherent states  $|\alpha\rangle$ . The coherent state  $|\alpha\rangle$  satisfies  $\hat{a}|\alpha\rangle = \alpha|\alpha\rangle$  where  $\alpha$  is a complex number. Here the phase-space coordinates  $\lambda$  are the real coordinates  $x$  and  $p$ , given by  $\alpha = (x + ip)/2$ . The single-mode  $Q$  function defines the quantum state  $|\psi\rangle$  uniquely as a positive probability distribution [98] and is normalized with respect to integration over the  $x, p$  variables.

The moments evaluated from the  $Q$  function distribution are antinormally ordered operator moments. It will be useful to write the variances in terms of antinormally ordered products [103]. The antinormal ordering of  $\hat{x}^2$  is given by

$$\langle \{\hat{x}^2\} \rangle = \langle \hat{x}^2 + 1 \rangle = e^{2gt} \langle \hat{x}^2(0) \rangle + 1. \quad (3.7)$$

Hence, if  $\sigma_x^2(t) = \langle \{\hat{x}^2(t)\} - \bar{x}^2 \rangle$  is the antinormally ordered variance, then

$$\sigma_x^2(t) = 1 + e^{2gt} \langle \hat{x}^2(0) - \bar{x}^2 \rangle = 1 + e^{2gt} (\sigma_x^2(0) - 1), \quad (3.8)$$

and similarly,

$$\sigma_p^2(t) = \langle \{\hat{p}^2(t)\} - \bar{p}^2 \rangle = 1 + e^{-2gt} (\sigma_p^2(0) - 1). \quad (3.9)$$

The antinormally ordered variances  $\sigma_x^2(t)$  and  $\sigma_p^2(t)$  are precisely the variances of  $x$  and  $p$  as defined by the  $Q$  function  $Q(x, p, t)$ .

### C. The superposition state

We will consider a measurement on the system prepared at time  $t_0$  in the superposition  $|\psi_{sup}\rangle = \sum_i c_i |x_i\rangle$ , where  $|x_j\rangle$  is an eigenstate of  $\hat{x}$  of the “position” quadrature with eigenvalue  $x_j$ . Applying the definition (3.6) and using the overlap function [102]

$$\langle x_j | \alpha \rangle = \frac{1}{\pi^{1/4}} \exp\left(-\frac{(x - x_j)^2}{4} + \frac{i}{2}p(x_j - 2x)\right), \quad (3.10)$$

the  $Q$  function for this state is given by

$$Q(x, p) = \frac{1}{\pi\sqrt{\pi}} \left| \sum_j c_j e^{-\frac{1}{4}(x - x_j)^2} e^{i\frac{p}{2}(x_j - 2x)} \right|^2. \quad (3.11)$$

This is a sum of Gaussians centered at each eigenvalue  $x_j$  along with additional interference cross-terms.

For the sake of simplicity without losing the essential features, we examine the simple superposition

$$|\psi_{sup}\rangle = c_1 |x_1\rangle + c_2 |-x_1\rangle. \quad (3.12)$$

We have also taken, without loss of the essential features,  $x_2 = -x_1$ . Here the  $c_j$  are complex amplitudes satisfying  $|c_1|^2 + |c_2|^2 = 1$ . The  $Q$  function simplifies to

$$Q_{sup}(x, p) \sim |c_1|^2 e^{-(x_1 - x)^2/2} + |c_2|^2 e^{-(x_1 + x)^2/2} - 2c_1 |c_2| e^{-x_1^2/2} e^{-x^2/2} \sin(x_1 p) \quad (3.13)$$

where we take  $c_1$  as real and  $c_2 = i|c_2|$ . A different choice of the phase of  $c_2$  introduces an unimportant phase shift in the sinusoidal term. The  $Q$  function for the superposition differs from the  $Q$  function,  $Q_{mix}(x, p)$ , for the mixture of eigenstates,

$$\rho_{mix} = \frac{1}{2} \{ |x_1\rangle\langle x_1| + |x_2\rangle\langle x_2| \}, \quad (3.14)$$

only by the addition of the third term corresponding to fringes. Without a momentum cutoff of  $|p| \leq p_m \gg 1$ , the distribution  $Q_{sup}(x, p)$  is not normalizable, as usual with pure position eigenstates in quantum mechanics. Since the limiting two-dimensional  $Q$  function cannot be normalized due to the infinite variance in  $\hat{p}$ , in the last line of (3.13) we have written the normalized projection along the  $x$  axis for a given  $p$ .

To obtain a more physical solution for (3.12), we model the position eigenstates as highly squeezed states in  $\hat{x}$ . The squeezed state is defined by [99]

$$|\beta_j, z\rangle_{sq} = D(\beta_j) S(z) |0\rangle. \quad (3.15)$$

Here,  $|0\rangle$  is the vacuum state satisfying  $\hat{a}|0\rangle = 0$ , and  $D(\beta_j) = e^{\beta_j \hat{a}^\dagger - \beta_j^* \hat{a}}$  and  $S(z) = e^{\frac{1}{2}(z^* \hat{a}^2 - z \hat{a}^{\dagger 2})}$  are the displacement and squeezing operators respectively, where  $z$  and  $\beta_j$  are complex numbers. For the state with squeezed fluctuations in  $\hat{x}$ , we note that  $z = r$  is a real and positive number that determines the amount of squeezing in  $\hat{x}$ . Defining  $\bar{x} = \langle \hat{x} \rangle$ ,  $\bar{p} = \langle \hat{p} \rangle$ , we find  $\langle (\Delta \hat{x})^2 \rangle = \langle \hat{x}^2(t) - \bar{x}^2 \rangle = e^{-2r}$ ,  $\langle (\Delta \hat{p})^2 \rangle = \langle \hat{p}^2(t) - \bar{p}^2 \rangle = e^{2r}$  and  $\langle \hat{a} \rangle = (\bar{x} + i\bar{p})/2 = \beta_j$ . We write  $\beta_j = (x_j + ip_j)/2$  where  $x_j$  and  $p_j$  are real. A position eigenstate  $|x_j\rangle$  is thus a squeezed state with  $r \rightarrow \infty$ . We take  $x_1$  and  $x_2$  real, so that with  $p_j = 0$ . The superposition (3.12) then becomes the superposition of two squeezed states

$$|\psi_{sup}(r)\rangle = c_1 |x_1, r\rangle_{sq} + c_2 |-x_1, r\rangle_{sq}. \quad (3.16)$$

We select  $c_2 = i|c_2|$  for convenience so that the normalization procedure gives the above form for all values of  $r$  and  $x_1$ . Otherwise, the normalization involves an extra term which vanishes in the limit where the two states forming the superposition are orthogonal. Here, this requires large  $r$ , i.e.  $r \rightarrow \infty$ .

The  $Q$  function for the squeezed state (3.15) is

$$Q(x, p) = \frac{1}{2\pi\sigma_x\sigma_p} e^{-(x-x_0)^2/2\sigma_x^2} e^{-(p-p_0)^2/2\sigma_p^2}, \quad (3.17)$$

where  $\sigma_x^2 = 2(1 + \tanh r)^{-1}$  and  $\sigma_p^2 = 2(1 - \tanh r)^{-1}$ . Here,  $\sigma_x^2$  and  $\sigma_p^2$  are the variances of  $x$  and  $p$  for the  $Q$  function distribution, which are given as

$$\begin{aligned} \sigma_p^2 &= 1 + e^{2r} \\ \sigma_x^2 &= 1 + e^{-2r}. \end{aligned} \quad (3.18)$$

This is in agreement with the *different* variances  $\langle (\Delta \hat{x})^2 \rangle = e^{-2r}$  and  $\langle (\Delta \hat{p})^2 \rangle = e^{2r}$  for the squeezed state (3.15), once antinormal ordering is accounted for.

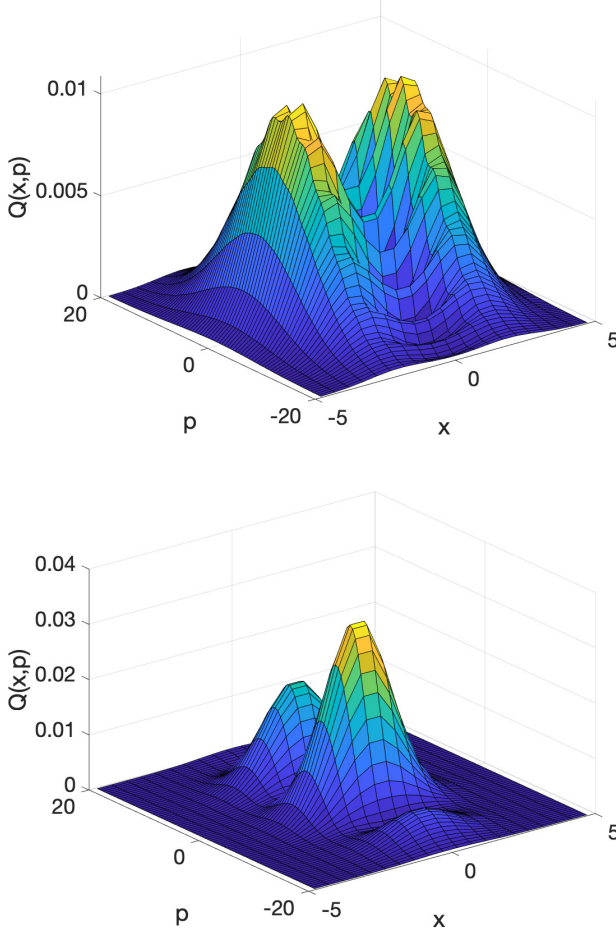


Figure 2. The analytic  $Q$  function for the superposition  $|\psi_{sup}\rangle$  of two eigenstates of  $\hat{x}$ . In fact we show (3.19) for  $r = 2$  and using  $x_2 = -x_1$ . The upper plot is for  $|x_1 - x_2| = 4 \gg 1$ . The lower plot is for  $|x_1 - x_2| = 1$ , so the  $x$  values are almost the same, but there are strong interference fringes in the complementary variable  $p$ .

Without losing essential features, we consider  $|\psi_{sup}\rangle$  with two states  $|\pm x_1, r\rangle$ , where  $r$  indicates the level of squeezing, and let  $c_1$  be real and  $c_2 = i|c_2|$ . The full  $Q$  function for (3.16) is

$$Q_{sup}(x, p) = \frac{e^{-p^2/2\sigma_p^2}}{4\pi\sigma_x\sigma_p} \left\{ |c_1|^2 e^{-(x-x_1)^2/2\sigma_x^2} + |c_2|^2 e^{-(x+x_1)^2/2\sigma_x^2} - 2|c_1 c_2| e^{-(x^2+x_1^2)/2\sigma_x^2} \sin(px_1/\sigma_x^2) \right\}, \quad (3.19)$$

where  $\sigma_x^2 = 1 + e^{-2r}$ , and  $\sigma_p^2 = 1 + e^{2r}$ . In the limit of  $r \rightarrow \infty$  where the system becomes the superposition  $|\psi_{sup}\rangle$  of two eigenstates, the  $Q$  function has two Gaussian peaks with fixed variance  $\sigma_x^2 = 1$ , centered at the eigenvalues  $x_1$  and  $x_2$ , along with a central peak centered at  $\bar{x} = 0$

whose amplitude has a fringe pattern which is damped by a term  $e^{-x_1^2/2}$ . Plots are shown in Figure 2.

#### D. Evolution: measurement dynamics

In the following sections, we will solve for trajectories  $x(t)$  and  $p(t)$  as the measurement of  $\hat{x}$  evolves (Figure 1). However, much can be inferred from the evolution of the  $Q$  function alone. We give a brief summary.

The  $Q$  function evolves according to  $H_A$  to give a final  $Q$  distribution which is calculable: The probability for observing  $x$  at the final time  $t_f$  is

$$P(x, t_f) \rightarrow |c_1|^2 e^{-(x-Gx_1)^2/2} + |c_2|^2 e^{-(x-Gx_2)^2/2} \quad (3.20)$$

where  $G = e^{|g|t}$ . This gives two sharp peaks located at  $Gx_1$  and  $Gx_2$  respectively, with relative probabilities  $|c_1|^2$  and  $|c_2|^2$ . The values  $x_i$  which correspond to the means of the Gaussians in (3.11) and (3.13) are *amplified* according to

$$x_j \rightarrow X_j = e^{gt} x_j \quad (3.21)$$

and are therefore ultimately observed; see the top plot of Figure 1. The means of the Gaussians correspond to the eigenvalues  $x_j$ , which are the results of the measurement.

In the amplification process  $H_A$ , the interference terms appearing in (3.11) and (3.13) are attenuated because of the proportionality to terms  $e^{-x_j^2}$ , which decay on amplification of  $x_j$  where  $x_j \rightarrow e^{gt} x_j$ . The measurement of  $\hat{x}$  amplifies the  $x_j$  variables, but attenuates the  $p$  variables to the minimum possible level of the vacuum (the lower plot of Figure 1). The complementary observable  $p$  therefore does not appear in the final measured probability. The inferred  $x_j$  at the time  $t_f$  therefore have a final probability distribution

$$P(x_j) = P(x_j, t_f) = |\langle x_j | \psi \rangle|^2, \quad (3.22)$$

in agreement with the quantum prediction.

While the eigenvalues  $x_j$  are amplified, the noise about these values is *not* amplified. Hence, the vacuum fluctuation  $x_\delta = x - x_j$  is not measurable, and does not lead to a macroscopic value. The values for these trajectories are determined by a *future* boundary condition [43, 53], implying retrocausality as shown in Figure 1.

It is also necessary to consider the measurement of the observable  $\hat{p}$ . The  $\hat{p}$  measurement takes place by amplifying  $p_j$ , using  $H_A$  with  $g < 0$ . We will show in Section V.F that for  $|\psi_{sup}\rangle$  the probability for observing  $p$  at the time  $t_f$  after evolution is

$$P(p, t_f) \rightarrow 1 - \sin[pe^{-|g|t}(x_1 - x_2)], \quad (3.23)$$

which gives a fringe pattern in the *amplified variable*  $Gp$ . This is in agreement with the quantum prediction for the measurement  $\hat{p}$ ,

$$P(p_j) = P(p_j, t_f) = |\langle p_j | \psi_{sup} \rangle|^2, \quad (3.24)$$

as it is inferred after taking into account the amplification by the measurement process. Here,  $|p\rangle$  is the eigenstate of  $\hat{p}$ .

#### IV. Q MODEL FOR STOCHASTIC DYNAMICS

We now analyze the measurement using the  $Q(x, p, t)$  function model, by deriving the forward-backward equations that determine the dynamics of the amplitudes  $\lambda = (x, p)$ . This requires rigorous proof of the connection between the stochastic equations for  $x(t)$  and  $p(t)$  and the Fokker-Planck equation governing the evolution of  $Q$ , under the interaction  $H_A$ .

##### A. Stochastic model: background

The  $Q$  function probability density  $Q(\lambda, t)$  for a phase-space coordinate  $\lambda$  is defined with respect to a non-orthogonal operator basis  $\hat{\Lambda}(\lambda)$  as

$$Q(\lambda, t) \equiv \text{Tr} \left( \hat{\Lambda}(\lambda) \hat{\rho}(t) \right), \quad (4.1)$$

where  $\rho$  is the density operator of the system. As  $Q(\lambda, t)$  is normalized to unity, it is necessary to normalize the basis so it integrates to unity, and the normalization condition is that  $\int \hat{\Lambda}(\lambda) d\lambda = \hat{1}$ . The basis satisfies  $\hat{\Lambda}^2(\lambda) = \mathcal{N}(\lambda) \hat{\Lambda}(\lambda)$ , which is different to the condition for projectors that  $\hat{P}^2 = \hat{P}$ , because it is a continuous non-orthogonal basis. From the Schrödinger equation, the dynamics of the probability distribution is obtained from the usual equation  $i\hbar d\hat{\rho}/dt = [\hat{H}, \hat{\rho}]$ . As a result, one obtains an equation for the  $Q$ -function time-evolution:

$$\frac{dQ(\lambda, t)}{dt} = \frac{i}{\hbar} \text{Tr} \left\{ [\hat{H}, \hat{\Lambda}(\lambda)] \hat{\rho}(t) \right\}. \quad (4.2)$$

This is equivalent to a zero-trace diffusion equation for the variables  $\lambda$ , of form  $\dot{Q}(\lambda, t) = \mathcal{L}(\lambda) Q(\lambda, t)$ , where  $\mathcal{L}(\lambda)$  is the differential operator for  $Q$ -function dynamics. While the examples given here are bosonic, such distributions can be extended to include fermions as well [100, 101, 104].

We can calculate directly how the  $Q$ -function evolves in time for a Hamiltonian  $H$ . To solve for single-mode evolution, we use the bosonic function  $Q(x, p) = \langle \alpha | \rho(t) | \alpha \rangle / \pi$  defined by eq (3.6) [98]. Here the phase-space coordinates  $\lambda$  are the real coordinates  $x$  and  $p$ , given by  $\alpha = (x + ip)/2$ .

We regard the  $Q$  function amplitudes  $\lambda$  ( $x$  and  $p$  in this paper) as representing a realization of the superposition state at the time  $t_0$ , immediately prior to the measurement, as well as during and after the measurement. The evolution of the  $Q$  function is given by equation (4.2). There is an equivalent time-symmetric stochastic action

principle for  $Q(\lambda, t)$ , leading to probabilistic path integrals [43]. These have sample trajectories  $\lambda$  that define the realistic path for all times.

The important step is to solve the dynamical  $Q$ -function equations for trajectories of the amplitudes  $\lambda$  ( $x$  and  $p$ ) with time as the measurement process evolves. For this purpose, we derive Theorems I and II below, allowing us to determine the stochastic dynamics. The Theorems prove the equivalence between the averages calculated from the amplitudes  $\lambda$  ( $x$  and  $p$ ) and those calculated from the  $Q$  function,  $Q(x, p)$ . This result is independently confirmed by statistical comparison for given simulations.

##### B. Conditional path integral equivalence theorem

###### 1. Definitions and notation

For  $M$  bosonic modes, the phase-space vector  $\lambda$  is a  $2M$ -dimensional real vector, and  $\mathbf{p}, \mathbf{x}$  are  $M$ -dimensional real vectors with  $\lambda = (\mathbf{x}, \mathbf{p})$ . The generalized Fokker-Planck equation (GFPE) satisfied by a  $Q$ -function is given by:

$$\dot{Q}(\lambda, t) = \mathcal{L}(\lambda) Q(\lambda, t). \quad (4.3)$$

The differential operator  $\mathcal{L}(\lambda)$  has both forward and backward components,

$$\mathcal{L}(\lambda) = \mathcal{L}_p(\mathbf{p}) - \mathcal{L}_x(\mathbf{x}), \quad (4.4)$$

where  $\mathcal{L}_{p,x}$  are defined as:

$$\mathcal{L}_p = \sum_j \left[ -\partial_j^p a_p^j(\mathbf{p}) + \frac{1}{2} \partial_j^p \partial_j^p d^j \right]. \quad (4.5)$$

Here  $\mathcal{L}_x$  is identical to  $\mathcal{L}_p$  except for the substitution of  $x$  for  $p$ , and we define  $\partial_j^p \equiv \partial/\partial p^j$ ,  $\partial_j^x \equiv \partial/\partial x^j$ . For the meter Hamiltonians in this paper, we have  $\mathbf{a}_p = \mathbf{a}_p(\mathbf{p})$  and  $\mathbf{a}_x = \mathbf{a}_x(\mathbf{x})$ , with diagonal diffusion  $\mathbf{d}$ .

We define the total action as:  $S_{kn} = S_{kn}^p + S_{kn}^x = \sum_{m=k+1}^n S_m$ . The “one-step” action for the  $n$ -th step is given by  $S_n = S_n^p + S_n^x$ , with  $S_n^p$  having the same form as  $S_n^x$  except for the changed superscripts:

$$S_n^p = S^p(\lambda_{n-1}, \lambda_n) = \sum_j \left[ \frac{\epsilon}{2d^j} |v_n^{j,p}|^2 + \ln(\sqrt{\mathcal{N}^j}) \right]. \quad (4.6)$$

The normalization factor is  $\mathcal{N}^j = (2\pi\epsilon d^j)$ , and the relative velocity fields  $\mathbf{v} \equiv (\mathbf{v}^p, \mathbf{v}^x)$  in the action are functions of neighboring coordinates:

$$\begin{aligned} \mathbf{v}_n^p &\equiv \frac{1}{\epsilon} (\mathbf{p}_n - \mathbf{p}_{n-1}) - \mathbf{a}^p(\mathbf{p}_{n-1}) \\ \mathbf{v}_n^x &\equiv \frac{1}{\epsilon} (\mathbf{x}_{n-1} - \mathbf{x}_n) - \mathbf{a}^x(\mathbf{x}_n). \end{aligned} \quad (4.7)$$



The two-time propagator  $G$  is then defined as:

$$G(\boldsymbol{\lambda}, t_k | \tilde{\boldsymbol{\lambda}}, \tilde{t}) = \lim_{\epsilon \rightarrow 0} \int \delta(\boldsymbol{\lambda} - \boldsymbol{\lambda}_k) \delta(\tilde{\boldsymbol{\lambda}} - \boldsymbol{\lambda}_{0N}) \mathcal{P}[\boldsymbol{\lambda}] d\boldsymbol{\lambda}. \quad (4.8)$$

Here,  $d\boldsymbol{\lambda} = \prod_{n=0}^N d\boldsymbol{\lambda}_n = \prod_{n=0}^N \prod_{k=1}^M dx_n^k dp_n^k$ ,  $\boldsymbol{\lambda}_{0N} = (\boldsymbol{x}_N, \boldsymbol{p}_0)$ , while  $\tilde{\boldsymbol{\lambda}} = (\boldsymbol{x}_f, \boldsymbol{p}_i)$  gives the initial momentum  $\boldsymbol{p}_i$  and final position  $\boldsymbol{x}_f$  at times  $\tilde{t} = (t_i, t_f) = (t_0, t_N)$ . The  $N$ -step total path probability  $\mathcal{P}$  for a path  $\boldsymbol{\lambda} = (\boldsymbol{\lambda}_0, \dots, \boldsymbol{\lambda}_N)$  at times  $t_k = t_0 + k\epsilon$ , with  $k = 0, \dots, N$ , is

$$\mathcal{P}[\boldsymbol{\lambda}] = e^{-S_{0N}}. \quad (4.9)$$

Marginals have the notation  $P(\boldsymbol{x}, t) = \int Q(\boldsymbol{\lambda}, t) d\boldsymbol{p}$ , with the variables that are integrated removed from the arguments. Boundary conditions are imposed on the final marginal  $P(\boldsymbol{x}, t_f)$  and initial conditional,  $P(\boldsymbol{p} | \boldsymbol{x}, t_i) = Q(\boldsymbol{\lambda}, t_i) P^{-1}(\boldsymbol{x}, t_i)$ .

## 2. Theorem I:

Any path-integral Q-function  $Q_{pi}$  obtained from multiplication by the joint probabilities at the boundaries satisfies the Q-function dynamical equations, where:

$$Q_{pi}(\boldsymbol{\lambda}, t) = \int G(\boldsymbol{\lambda}, t | \tilde{\boldsymbol{\lambda}}, \tilde{t}) P(\tilde{\boldsymbol{\lambda}}, \tilde{t}) d\tilde{\boldsymbol{\lambda}}. \quad (4.10)$$

The quantum Q-function solution,  $Q = Q_{pi}$  is found on solving *simultaneous equations for the joint distribution*  $P(\tilde{\boldsymbol{\lambda}}, \tilde{t})$ , and hence for  $Q_{pi}$ , where:

$$\int Q_{pi}(\boldsymbol{\lambda}, t_f) d\boldsymbol{p} = P(\boldsymbol{x}, t_f), \quad (4.11)$$

and:

$$\frac{Q_{pi}(\boldsymbol{\lambda}, t_i)}{\int Q_{pi}(\boldsymbol{\lambda}, t_i) d\boldsymbol{p}} = P(\boldsymbol{p} | \boldsymbol{x}, t_i). \quad (4.12)$$

*Proof:*

We wish to show that  $Q_{pi} = Q$ , by proving that  $Q_{pi}$  satisfies the GFPE (4.3), and has an initial condition that corresponds to the Q-function for the initial quantum state. From linearity, proving that  $Q_{pi}(\boldsymbol{\lambda})$  satisfies the GFPE 4.3 is achieved by verifying this for the propagator,  $G(\boldsymbol{\lambda}, t | \tilde{\boldsymbol{\lambda}}, \tilde{t})$ . To show this, define advanced and retarded propagators for  $\boldsymbol{\lambda}$  at  $t = t_j$  with  $\tilde{\boldsymbol{p}} = \boldsymbol{p}_0$  at  $t_i = t_0$  and  $\tilde{\boldsymbol{x}} = \boldsymbol{x}_N$  at  $t_f = t_N$ , as

$$G^r(\boldsymbol{p}_j, t | \tilde{\boldsymbol{p}}, t_i) = \lim_{\epsilon \rightarrow 0} \int e^{-S_{0j}^p} \prod_{n=1}^{n-1} d\boldsymbol{p}_n, \\ G^a(\boldsymbol{x}_j, t | \tilde{\boldsymbol{x}}, t_f) = \lim_{\epsilon \rightarrow 0} \int e^{-S_{jN}^x} \prod_{n=j+1}^{N-1} d\boldsymbol{x}_n. \quad (4.13)$$

Due to its path-integral construction,  $G^r$  satisfies a forward Kolmogorov equation in  $\boldsymbol{p}$  [105, 106]. By reversing the sign of  $t$ , we find that  $G^a$  also satisfies a forward Kolmogorov equation in  $\boldsymbol{x}$ , but in the negative time direction:

$$\dot{G}^r(\boldsymbol{p}, t | \tilde{\boldsymbol{p}}, t_i) = \mathcal{L}^p G^r(\boldsymbol{p}, t | \tilde{\boldsymbol{p}}, t_i) \\ \dot{G}^a(\boldsymbol{x}, t | \tilde{\boldsymbol{x}}, t_f) = -\mathcal{L}^x G^a(\boldsymbol{x}, t | \tilde{\boldsymbol{x}}, t_f). \quad (4.14)$$

The normalization of the advanced Gaussian propagator terms in the path integral for  $\boldsymbol{x}_n$  with  $n < j$  means that all these past time factors integrate to unity. Similarly, the retarded propagator is independent of  $\boldsymbol{p}_n$  for future time points  $n > j$ , as these also integrate to give unity. As a result, we can write that:

$$G^r(\boldsymbol{p}, t_k | \tilde{\boldsymbol{p}}, t_0) = \lim_{\epsilon \rightarrow 0} \int e^{-S_{0N}^p} \delta(\boldsymbol{p} - \boldsymbol{p}_k) \delta(\tilde{\boldsymbol{p}} - \boldsymbol{p}_0) d\boldsymbol{p}, \\ G^a(\boldsymbol{x}, t_k | \tilde{\boldsymbol{x}}, t_f) = \lim_{\epsilon \rightarrow 0} \int e^{-S_{0N}^x} \delta(\boldsymbol{x} - \boldsymbol{x}_k) \delta(\tilde{\boldsymbol{x}} - \boldsymbol{x}_N) d\boldsymbol{x}. \quad (4.15)$$

From these results and the definitions above, it follows that the total propagator factorizes as  $G(\boldsymbol{\lambda}, t | \tilde{\boldsymbol{\lambda}}, \tilde{t}) = G^r(\boldsymbol{p}, t | \tilde{\boldsymbol{p}}, t_0) G^a(\boldsymbol{x}, t | \tilde{\boldsymbol{x}}, t_f)$ . Hence, using the chain rule for differentiation and Eq (4.14), the required time-evolution can be written as:

$$\dot{G}(\boldsymbol{\lambda}, t | \tilde{\boldsymbol{\lambda}}) = \dot{G}^r(\boldsymbol{p}, t | \tilde{\boldsymbol{p}}, t_0) G^a(\boldsymbol{x}, t | \tilde{\boldsymbol{x}}, t_f) \\ + G^r(\boldsymbol{p}, t | \tilde{\boldsymbol{p}}, t_0) \dot{G}^a(\boldsymbol{x}, t | \tilde{\boldsymbol{x}}, t_f) \\ = (\mathcal{L}^p - \mathcal{L}^x) G(\boldsymbol{\lambda}, t | \tilde{\boldsymbol{\lambda}}, \tilde{t}). \quad (4.16)$$

Due to linearity, any integral of  $G$  over its boundary values also satisfies the GFPE. Therefore, the path integral construction must obey the required GFPE,

$$\dot{Q}_{pi}(\boldsymbol{\lambda}, t) = (\mathcal{L}_p(\boldsymbol{p}) - \mathcal{L}_x(\boldsymbol{x})) Q_{pi}(\boldsymbol{\lambda}, t). \quad (4.17)$$

Provided the joint probability  $P(\tilde{\boldsymbol{\lambda}}, \tilde{t})$  satisfies the boundary equations, one can verify that at the initial time,  $Q_{pi}(\boldsymbol{\lambda}, t_0) = Q(\boldsymbol{\lambda}, t_0)$ . Due to uniqueness of the solutions to a first order differential equations,  $Q_{pi}$  is equal to the quantum-mechanical Q-function solution for all times.

As a further check, in the short-time limit of  $t_0 = t_f$  we find that

$$\lim_{t_0, t_f \rightarrow t} G(\boldsymbol{\lambda}, t | \tilde{\boldsymbol{\lambda}}) = \delta(\boldsymbol{\lambda} - \tilde{\boldsymbol{\lambda}}), \quad (4.18)$$

hence, as  $t_0, t_f \rightarrow t$ , one has that:

$$\lim_{t_0, t_f \rightarrow t} Q_{pi}(\boldsymbol{\lambda}, t) = \int \delta(\boldsymbol{\lambda} - \tilde{\boldsymbol{\lambda}}) P(\tilde{\boldsymbol{\lambda}}, t') d\tilde{\boldsymbol{\lambda}}, \\ = P(\boldsymbol{p} | \boldsymbol{x}, t') P(\boldsymbol{x}, t'). \quad (4.19)$$

From the definition of the conditional probability, this is the initial Q-function.



### 3. Theorem II:

The path-integral solution corresponds to a time-symmetric stochastic differential equation (TSSDE) with a specified conditional initial distribution in  $\mathbf{p}$  and final marginal distribution in  $\mathbf{x}$  :

$$\begin{aligned} p^j(t) &= p^j(t_0) + \int_0^t a_p^j(t') dt' + \int_0^t dw_p^j \\ x^j(t) &= x^j(t_f) + \int_t^{t_f} a_x^j(t') dt' + \int_t^{t_f} dw_x^j. \end{aligned} \quad (4.20)$$

Here  $\mathbf{x}(t_f)$  is distributed as  $P(\mathbf{x}, t_f)$ , while  $\mathbf{p}(t_0)$  is distributed conditionally as  $C(\mathbf{p}|\mathbf{x}(t_0), t_0)$ , and  $[dw^\mu] = (d\mathbf{w}_x, d\mathbf{w}_p)$  are independent real Gaussian noises correlated as

$$\langle dw^\mu dw^\nu \rangle = \delta^{\mu\nu} d^\mu \epsilon, \quad (4.21)$$

where  $\mu = 1, 2M$  and  $d^{j+M} = d^j$ .

*Proof:*

The TSSDE is obtained by discretizing the equation for times  $t_k = t_0 + k\epsilon$ , with  $k = 0, \dots, N$ , and then taking the limit of  $\epsilon \rightarrow 0$ . We define  $[\lambda] = [\lambda_0, \lambda_1, \dots, \lambda_N]$  as the stochastic path. The discretized solutions are then given as the simultaneous solutions of the equations, for  $k = 1, \dots, N$

$$\begin{aligned} \mathbf{p}_k &= \mathbf{p}_{k-1} + \mathbf{a}^p(\mathbf{p}_{k-1})\epsilon + \Delta_k^p \\ \mathbf{x}_{k-1} &= \mathbf{x}_k + \mathbf{a}^x(\mathbf{x}_k)\epsilon + \Delta_k^x, \end{aligned} \quad (4.22)$$

To obtain an equivalent path integral to the TSSDE, we first obtain the  $N$ -step trajectory probability density, conditioned on random noises  $[\Delta]$ . This is a product of Dirac delta functions,

$$\mathcal{G}([\lambda] | [\Delta]) = \prod_{j=1}^n \delta^{2M}(\epsilon \mathbf{v}_j - \Delta_j), \quad (4.23)$$

which gives a normalized probability conditioned on a specific noise vector  $[\Delta]$ . Solving for the resulting set of trajectory values  $[\lambda]$  that satisfy the delta-function constraints is straightforward in the parametric amplifier case, due to the decoupling of forward and backward equations.

In a Fourier transform representation with  $\mathbf{k}_j \equiv (k_j^1, k_j^2, \dots, k_j^{2M})$ , one can expand the delta-functions as

$$\mathcal{G}_n([\lambda] | [\Delta]) = \prod_{j=1}^n \int \frac{d\mathbf{k}_j}{(2\pi)^{2M}} e^{-i\mathbf{k}_j(\mathbf{v}_j \epsilon - \Delta_j)}. \quad (4.24)$$

The  $2M$  real Gaussian noises  $\Delta_k$  at each step in time, for  $k > 0$ , are distributed as:

$$P(\Delta_k) = \frac{1}{(2\pi\epsilon d)^M} e^{-|\Delta_k|^2/(2\epsilon d)}. \quad (4.25)$$

On integration over  $\mathbf{k}_j$  one obtains the path probability result as defined previously:

$$\mathcal{G}_n([\lambda]) = \int \mathcal{G}_n([\lambda] | [\Delta]) P([\Delta]) d[\Delta]. \quad (4.26)$$

By construction, the initial values of  $\mathbf{x}_N$  and  $\mathbf{p}_0$  are sampled according to the required joint and conditional probabilities. Hence the probability of a TSSDE solution is  $Q_{pi}$ , which is equal to the quantum average  $Q$  from Theorem I.

### C. Numerical $\chi^2$ tests

The analytic theorems obtained above were verified numerically using  $\chi^2$  tests in several cases described here. The forward-backward stochastic equations were integrated by first propagating  $x$  backwards in time, generating a conditional sample, then propagating  $p$  forwards in time.

All trajectories plotted use 40 sample trajectories, to provide an intuitive demonstration of how they behave. In order to verify the quantitative accuracy of the trajectory probability distributions, large numbers of samples were generated and plotted using binning methods.

These samples were statistically tested with  $\chi^2$  methods [107, 108] to compare them with analytic solutions. The test cases used  $N_s = 2 \times 10^6$  sample trajectories to obtain good statistics for the numerically sampled distributions,

$$p_{ijk}^{samp} = \frac{N_{ijk}}{N_s}. \quad (4.27)$$

Here  $N_{ijk}$  is the number of trajectories in the bin at  $x_i, p_j$ , and sampled time  $t_k$ . Such verification requires binning on a three-dimensional  $(x, p, t)$  grid, to obtain numerical estimates of the integrated analytic probabilities  $p_{ijk}$ , where:

$$p_{ijk} = \int_A d\delta x d\delta p Q(x_i + \delta x, p_j + \delta p, t_k). \quad (4.28)$$

This was evaluated by numerical integration of the analytic  $Q$  distribution, using a two-dimensional Simpson's rule integrator in each bin.

In order to treat the dynamics of the Q-function, time-averages were evaluated to give a definitive overall result. Due to the correlations inside each trajectory, the range of fluctuations of time-averaged statistics are reduced compared to one-time tests, which exactly follow the  $\chi^2$  distribution. Individual tests at each time-point are in agreement with  $\chi^2$  statistics, and will be reported elsewhere.

We therefore define:

$$\bar{\chi}^2 = \frac{1}{N_t} \sum_{i,j,k} \frac{\left\langle [p_{ijk} - p_{ijk}^{samp}]^2 \right\rangle}{\left\langle \sigma_{ijk}^2 \right\rangle}. \quad (4.29)$$

Here,  $\sigma_{ijk}^2 = p_{ijk}/N_s$  is the expected probability variance for  $N_s$  total samples and  $N_t$  time points, with a phase-space bin area of  $A$ .

As an example, the simulations described in Figure (3) used 30 time-steps of  $gdt = 0.1$ , combined with a midpoint stochastic integration method for improved accuracy [109]. No significant discretization error improvements were found with smaller time-steps. Comparisons were made between the analytic and numerically sampled  $Q(x, p, t)$  distributions with  $dx = 0.02$  and  $dp = 0.05$ . This gave an average of  $\sim 55,100$  comparison grid-points at each time step, after discarding bins with non-significant sample populations of  $N < 10$  [110].

In a typical test with  $2 \times 10^6$  sample trajectories and  $A = 10^{-3}$ , the time-averaged statistical error was  $\bar{\chi}^2 = 55.2 \times 10^3$ , with  $1.7 \times 10^6$  valid comparisons. There were an average of  $k = 55.1 \times 10^3$  significant points per time-step. This shows that  $\bar{\chi}^2$  is within the expected range of  $\langle \chi^2 \rangle = k \pm \sqrt{2k}$ .

Hence, as expected, there is good agreement between the analytic  $Q$ -function probability from quantum theory and the ensemble averaged stochastic trajectories.

## V. STOCHASTIC EQUATIONS AND SOLUTIONS

### A. Generalised Fokker-Planck equation for $Q$ function

For the system evolving according to the Hamiltonian  $H_A = \frac{i\hbar g}{2} [\hat{a}^{\dagger 2} - \hat{a}^2]$  given by (3.3), a dynamical equation for the  $Q$  function can be derived [53, 93]. Applying the correspondence rules to transform operators into differential operators, one obtains a generalized Fokker-Planck type equation in terms of complex coherent state variables  $\alpha$ :

$$\frac{dQ}{dt} = - \left[ g \frac{\partial}{\partial \alpha} \alpha^* + \frac{g}{2} \frac{\partial^2}{\partial \alpha^2} + h.c. \right] Q. \quad (5.1)$$

Using the quadrature definitions where the vacuum has unit noise in  $x$  and  $p$ , one has  $\alpha = (x + ip)/2$ , or  $\hat{x} = \hat{a} + \hat{a}^\dagger$ . We obtain

$$\frac{dQ}{dt} = [\partial_p (gp) - \partial_x (gx) + g (\partial_p^2 - \partial_x^2)] Q. \quad (5.2)$$

This demonstrates a diffusion matrix which is traceless and equally divided into positive and negative definite parts, and a drift matrix:

$$A = \begin{bmatrix} \dot{x} \\ \dot{p} \end{bmatrix} = \begin{bmatrix} gx \\ -gp \end{bmatrix}. \quad (5.3)$$

### B. Forward-backward stochastic equations

Using the above equivalence Theorem, we solve the measurement dynamics for the dynamics of  $H_A$ . Here,

the  $x$  and  $p$  dynamics decouple. However, to obtain a mathematically tractable equation for the traceless noise matrix, we follow [53] and the sign of  $t$  is reversed in the amplified dynamics of  $x$ .

The corresponding integrated stochastic equations for  $g > 0$  are:

$$\begin{aligned} p(t) &= p(t_0) - \int_{t_0}^t g p dt' + \int_{t_0}^t dw_p \\ x(t) &= x(t_f) - \int_t^{t_f} g x dt' + \int_t^{t_f} dw_x \end{aligned} \quad (5.4)$$

where  $\langle dw^\mu dw^\nu \rangle = 2g \delta^{\mu\nu} dt$ .

Alternatively, in differential form, we obtain [53, 93]

$$\frac{dp}{dt} = -gp + \sqrt{2g} \xi_p \quad (5.5)$$

with a boundary condition in the past, and

$$\frac{dx}{dt_-} = -gx + \sqrt{2g} \xi_x \quad (5.6)$$

with a boundary condition in the future, where  $t_- = -t$ . Defining  $\xi = (\xi_p, \xi_x) = [\xi^\mu]$ , the Gaussian random noises  $\xi^\mu(t)$  satisfy:  $\langle \xi^\mu(t) \xi^\nu(t') \rangle = \delta^{\mu\nu} \delta(t - t')$ . Thus, there is a forward-backward stochastic differential equation (FBSDE), for individual trajectories. This describes two individual stochastic trajectories, such that the average of the dynamical trajectories equals the  $Q$ -function averages. The trajectories are decoupled dynamically, with decay and stochastic noise occurring in each of the time directions. One propagates forward, and one backwards in time.

This leads us to consider a case where the trajectory in  $x$  has a future marginal,  $P(x, t_f)$ . The trajectory in  $p$  has a past conditional distribution,  $P(p|x, t_0)$ , which depends on  $x$  in the future (Figures 1 and 3), giving cyclic causal behavior.

### C. Causal consistency

There is a Grandfather-type paradox arising from the present seemingly depending on the future. This will be examined later in Section VII by proposing a causal model based on the simulations, in which the retrocausal trajectory  $x(t)$  contributes noise at a microscopic level only (Figures 1 and 3).

However, the significant result of causal consistency is proved by the Theorems I and II: The quantum state  $|\psi\rangle$  as determined uniquely by the  $Q$  function  $Q(x, p, t)$  depends *only* on the time  $t$  of evolution, starting from the initial time  $t = 0$ . This is despite that the trajectory  $x(t)$  depends on the future boundary, which can be an arbitrary infinite time  $t_f$  in the future. The adjustment of the future time  $t_f$  cannot change the quantum state  $Q$  at the time  $t$ . Similar consistencies are well known in absorber theory for electromagnetic fields [6, 7, 14] and

in theories of closed timelike curves [97]. The consistency ensures that the trajectories at large time  $t_f \rightarrow \infty$  satisfy the conditional relations connecting  $x(t_f)$  and  $p(t_f)$  for the amplified state, which quantifies the end part of the loop.

#### D. Measuring $\hat{x}$ : A system in a superposition of eigenstates of $\hat{x}$

To solve the trajectories for the field amplitudes, we stochastically sample according to the noise terms  $\xi^\mu(t)$ . From Eq. (5.6), we see that the  $x$  solution at  $t$  depends on the boundary condition for  $x$  imposed in the *future* final time  $t_f$ , after the measurement has been completed. We solve this equation first, by propagating the trajectories for  $x$  backwards in time. We refer to these trajectories as backward trajectories.

For sufficiently amplified fields  $x$ , we justify modeling the final stage of measurement as a direct detection of the amplified amplitude  $x$  at  $t_f$ . This model is justified because the amplitudes for  $x$  at the final time have a distribution given by the final  $Q$  function,  $P(x, t_f)$ , which one can show is precisely that corresponding to the quantum prediction  $P_{sup}(x, t_f) \rightarrow P(x) = |\langle x | \psi_{sup} \rangle|^2$ , as  $t_f \rightarrow \infty$ . We proved this for a superposition of  $\hat{x}$  eigenstates in Section III, and illustrate further by examples below, and in Section V.G. To evaluate the sampling distribution for the future boundary at time  $t_f$ , we evaluate the evolving  $Q$  function  $Q_{sup}(x, p, t)$  at the time  $t = t_f$ , from the Hamiltonian  $H_A$  of (3.3) that amplifies  $\hat{x}$ . The original  $Q$  function in the present time  $t_0$  is given by (3.19). We evaluate the  $Q$  function for the amplified system with respect to  $x$ , *after* the measurement  $H_A$  has acted for a time  $t$ . This calculation can be done in two ways. The state formed after the unitary evolution  $H_A$  is  $e^{-iH_A t/\hbar} |\psi_{sup}(r)\rangle$ , for which the  $Q$  function can be evaluated directly as

$$Q_{sup}(x, p, t) = \frac{e^{-p^2/2\sigma_p^2(t)}}{4\pi\sigma_x(t)\sigma_p(t)} \left\{ |c_1|^2 e^{-(x-G(t)x_1)^2/2\sigma_x^2(t)} + |c_2|^2 e^{-(x+G(t)x_1)^2/2\sigma_x^2(t)} - 2|c_1||c_2| e^{-(x^2+G^2(t)x_1^2)/2\sigma_x^2(t)} \times \sin\left(\frac{pG(t)x_1}{\sigma_x^2(t)}\right) \right\}. \quad (5.7)$$

Here  $G(t) = e^{gt}$  is the amplification factor, and the variances becomes

$$\sigma_{x/p}^2(t) = 2(1 \pm \tanh(r - gt))^{-1} = 1 + e^{\pm 2(gt-r)}. \quad (5.8)$$

The solutions can also be found from the dynamical equation (4.2) for the  $Q$  function. We denote the  $Q$  function at the future time  $t = t_f$  as  $Q_{sup}(x, p, t_f)$ .

Due to the separation of variables  $x$  and  $p$  in Eqs. (5.5)-(5.6), the marginal distribution  $P_{sup}(x, t_f) = \int Q_{sup}(x, p, t_f) dp$  for  $x$  at the future time  $t = t_f$  determines the initial sampling distribution for the backward

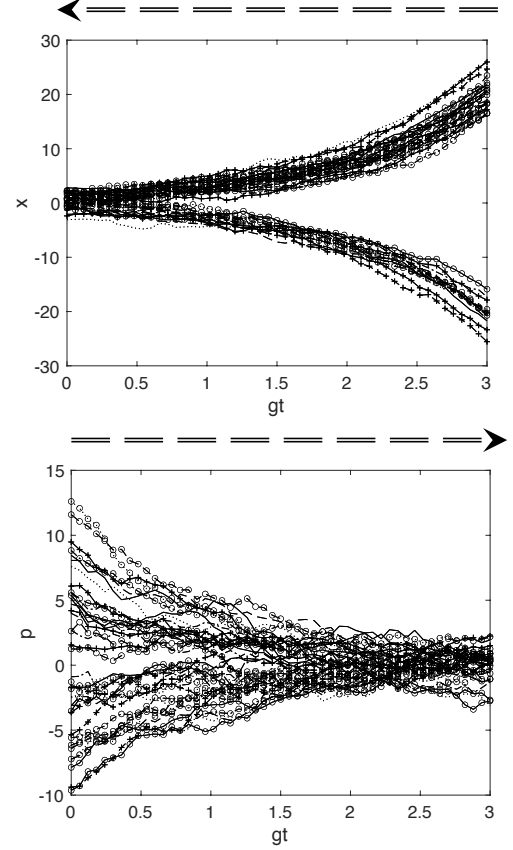


Figure 3. Measurement of  $\hat{x}$  on a system prepared in a superposition  $|\psi_{sup}\rangle$  of two eigenstates  $|x_1\rangle$  and  $|x_2\rangle$ . The top plot shows trajectories for  $x$  as the system evolves for a time  $t$  according to  $H_A$  which amplifies  $\hat{x}$ . Here,  $x_1 = -x_2 = 1$ , so that  $|\psi_{sup}\rangle$  models a microscopic superposition. The trajectories originating from the boundary at  $t_f = 3/g$  are sampled from a distribution that is a 50/50 mixture of two Gaussians, with means  $e^{gt}x_1$  and  $-e^{gt}x_1$ , and variance  $\sigma_x^2 = 1$ . The trajectories propagate backwards from the future boundary at  $gt = 3$ , from either  $e^{gt}$  or  $-e^{gt}$  ( $g > 0$ ), but subject to noise  $\xi_x(t)$  with variance at the vacuum level,  $\sigma_x^2 = 1$ . The noise is not amplified or attenuated. The lower plot shows the forward-propagating trajectories for the complementary variable  $p$ . Here, the values are attenuated to the vacuum noise level,  $\sigma_p^2 = 1$ . We take the superposition (3.16) with  $r = 2$ .

$x$  trajectories. The sampling is determined by the future marginal and is *identical to the case of the system prepared in a mixture of eigenstates*,  $\rho_{mix}$ , (Eq. (3.14)), because the interference terms associated with the superposition *do not amplify*. The procedure of the simulation hence implies a *forward causal relation*. The initial  $Q$  function at time  $t_0$  involves a set of Gaussians with means corresponding to the eigenvalues  $x_j$ . The final  $Q$  function at time  $t_f$  directly follows from the initial  $Q$  function, with the means being amplified to  $Gx_j$ . This is depicted by the forward causal relation given by the solid blue line in Figures 1 and 4. The marginal for  $x$  at

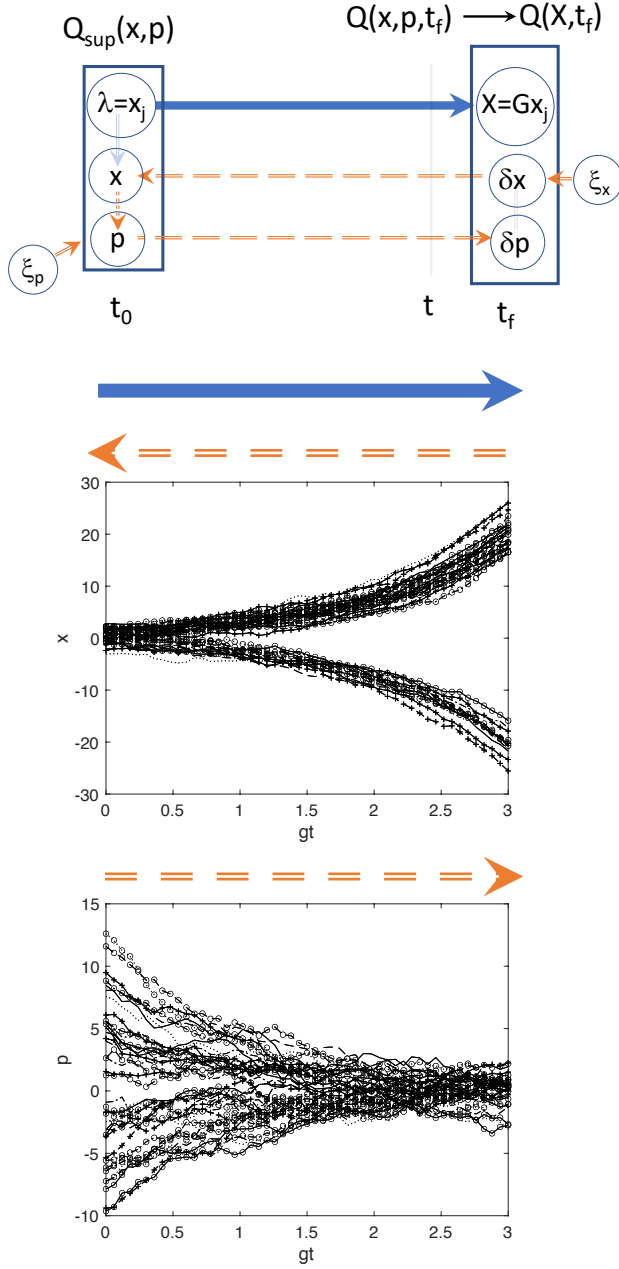


Figure 4. Causal relations for the simulation of a measurement  $\hat{x}$  on the system in the superposition  $|\psi_{sup}\rangle$  of eigenstates  $|x_j\rangle$  of  $\hat{x}$ . The simulation is described in Figure 3. The arrows imply the direction of cause and effect and the direction from left to right is the direction of time. Here,  $X$  is the outcome for the measurement  $\hat{x}$ . The rectangle represents the system, which is described by the  $Q$  function  $Q_{sup}(x, p)$  at time  $t_0$ . The solid blue arrow represents a deterministic causal relation where the eigenvalue  $\lambda = x_j$  for  $\hat{x}$  becomes the result  $G\lambda$  for  $X$  on the measurement  $\hat{x}$ , which gives amplification by a factor  $G = e^{g|t|}$ . The red dashed lines represent retrocausal (right to left) and causal (left to right) influences for  $x$  and  $p$ . The  $p$ ,  $\delta x$  and  $\delta p$  are not amplified and hence not measured. The conditional distribution  $P_Q(p|x)$  at the boundary  $t_0$  determines the correlation between  $x$  and  $p$  at  $t_0$ , which ensures connection between forward and backward trajectories. The trajectories are consistent with the moments of  $Q_{sup}(x, p, t)$  for each  $t$ . As  $t_f \rightarrow \infty$ , the  $x$  and  $p$  become uncorrelated, indicated by the grey line at the future boundary.

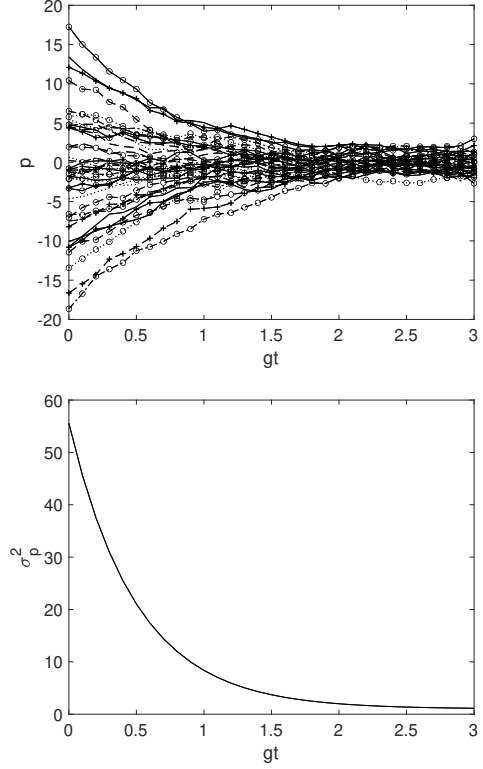


Figure 5. Measurement of  $\hat{x}$ . Plot of forward propagating trajectories for the attenuated variable  $p$  versus  $gt$  for the system prepared in a superposition  $|\psi_{sup}\rangle$  (Eq. (3.16)) of two position eigenstates, with  $r = 2$ , and  $x_1 = 1$ . The top plot shows trajectories with  $t_f = 3/g$ . The second plot shows the reduction in the variance  $\sigma_p^2$  to the value of 1.

the time  $t \geq t_0$  is

$$P_{sup}(x, t) = \frac{1}{\sqrt{2\pi}\sigma_x(t)} \left\{ |c_1|^2 e^{-(x-G(t)x_1)^2/2\sigma_x^2(t)} + |c_2|^2 e^{-(x+G(t)x_1)^2/2\sigma_x^2(t)} \right\}. \quad (5.9)$$

We note the variance can be written  $\sigma_x^2(t) = 1 + G^2(t) [\sigma_x^2(0) - 1]$  where  $G(t) = e^{gt}$ . We see that the marginal and hence the trajectories for the measured variable  $x$  are identical to those of  $\rho_{mix}$ .

The backward trajectories for  $r = 2$  are shown in Figures 1, 3 and 4, and are depicted by the backward relation shown by the dashed arrows in Figures 3 and 4. The important result is that regardless of the separation  $\sim |x_1|$  between the eigenvalues associated with the eigenstates  $|x_1\rangle$  and  $|-x_1\rangle$ , the eigenstates are always distinguishable upon measurement for large  $gt$ . This occurs in the limit of large squeezing,  $r \rightarrow \infty$ , where the squeezed states become eigenstates. The result arises because the hidden vacuum noise (given in Eq. (3.18) by  $\sigma_x = 1$ ) associated the  $Q$  function eigenstate (3.17) is *not* amplified by  $H_A$ . This feature ensures the realization of the measurement postulate and Born's rule, as we explain in Section V.G.

The forward trajectories for the attenuated variable

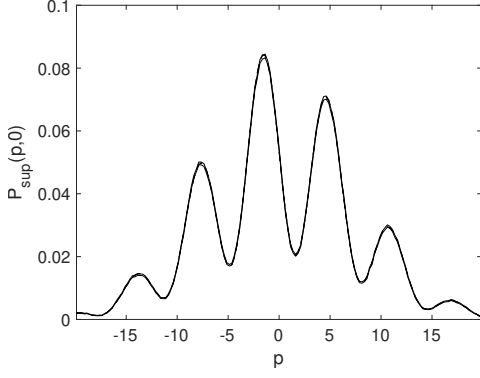


Figure 6. Measurement of  $\hat{x}$ . As in Fig (5), except showing the corresponding marginal  $P_{sup}(p, 0)$  for  $p$  at the *initial* time  $t = t_0 = 0$ , where fringes are evident due to quantum interference.

$p$  are shown in Figures 1, 3, 4 and 5. These are depicted in Figure 4 by the forward-going red dashed arrows. The trajectories are calculated by solving (5.5) using the boundary condition at time  $t_0 = 0$ , which we refer to as the past, or present, time. The forward and backward equations decouple, and hence it is the marginal  $P_{sup}(p, 0) = \int Q_{sup}(x, p) dx$  for  $p$  at time  $t_0 = 0$  that is relevant to the sampling. We find

$$P_{sup}(p, 0) = \frac{e^{-p^2/2\sigma_p^2}}{\sqrt{2\pi}\sigma_p} \left\{ 1 - e^{-x_1^2/2\sigma_x^2} \sin(px_1/\sigma_x^2) \right\}. \quad (5.10)$$

From this solution, we see that with increasing separation of the two eigenstates  $|x_1\rangle$  and  $|-x_1\rangle$  (so that  $|x_1|$  increases), the fringes become less prominent (compare with Figure 6). The evolution of  $P_{sup}(p, t)$  is shown in Figure 7. The trajectories decay to a level given by the vacuum noise, as shown in Figure 5.

Although they propagate independently, the forward and backward trajectories are linked according to the correlation given by  $Q(x, p, 0)$ , at the initial time. This is the origin of a causal loop (Figure 4) (refer Section VI.) For the mixture  $\rho_{mix}$ , there is no correlation. At every time  $t$  during the dynamics, the correlations between the trajectories match those of  $Q(x, p, t)$  (refer Section IV.C), giving causal consistency (grey line in Figure 4). The  $x$  and  $p$  become decorrelated in the limit as  $t_f \rightarrow \infty$ .

### E. Measuring $\hat{x}$ : A system in a cat state

It is interesting to simulate the measurement of  $\hat{x}$  on the system prepared in a superposition of two coherent states [102]

$$|cat\rangle = \frac{e^{-i\pi/4}}{\sqrt{2}} \{ |\alpha_0\rangle + e^{i\pi/2} |-\alpha_0\rangle \}, \quad (5.11)$$

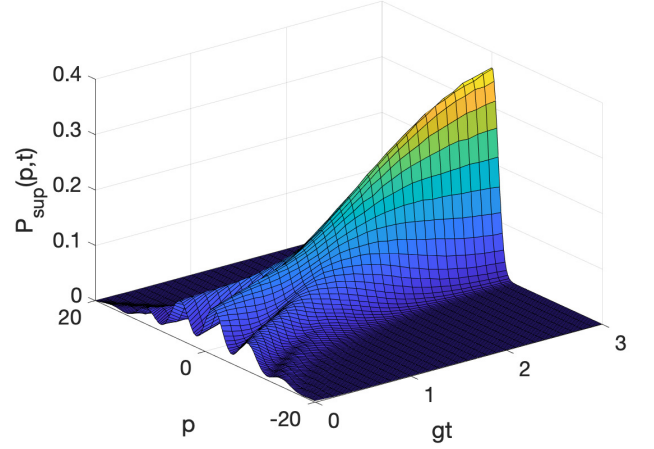


Figure 7. Measurement of  $\hat{x}$ . As for Figure 3, with  $r = 2$  and  $x_1 = 1$ . The plot shows the evolution of the distribution  $P_{sup}(p, t)$  for  $p$  as evaluated from  $10^6$  multiple trajectories, a sample of which is given in Figure 6. The fringes are evident at  $t = t_0 = 0$ .

which for large  $\alpha_0$  is the “cat state” [111]. This corresponds to  $r = 0$  in the expression (3.16), with  $x_1 = 2\alpha_0$ . We take  $\alpha_0$  real. The  $Q$  function is given by (3.16).

The quantum noise associated with the  $Q$  function for the coherent state  $|\alpha_0\rangle$  has *two* contributions: The first noise contribution is the “hidden” vacuum noise which exists for the eigenstate  $|x_1\rangle$  itself, and is *not* amplified. The second noise contribution corresponds to the *measured* vacuum noise level  $\langle(\Delta\hat{x})^2\rangle = 1$  of a coherent state. This noise level, being measurable, is *amplified* by the measurement interaction  $H_A$ , Eq. (3.3). The additional vacuum noise appears in the simulations as extra noise in the final amplified outputs at time  $t_f$ , evident from Figure 8.

We demonstrate the effectiveness of the model  $H_A$  for the measurement of  $\hat{x}$  by evaluating the final distribution  $P_{sup}(x, t_f)$ . The final marginal distribution  $P_{sup}(x, t_f)$  in the large amplification limit is given by (5.21), which corresponds to  $P_B(x) = |\langle x|cat\rangle|^2$  as predicted by quantum mechanics (Born’s rule). Here,  $|x\rangle$  is the eigenstate for  $\hat{x}$ . We see this analytically by noting that the marginal for  $x$  at large amplification where  $gt \rightarrow \infty$  can be written in terms of the scaled variable  $\tilde{x} = x/e^{gt}$  as

$$P_{sup}(\tilde{x}, t) = \frac{1}{2\sqrt{2\pi}} \left\{ e^{-(\tilde{x}-x_1)^2/2} + e^{-(\tilde{x}+x_1)^2/2} \right\}, \quad (5.12)$$

where here we use the result that  $\sigma_x^2(t) \rightarrow e^{2gt}$ . This agrees with  $P_B(x) = |\langle x|cat\rangle|^2$  as predicted by quantum mechanics, and evaluated in [102] using  $x_1 = 2\alpha_0$  (after correcting to deduce the inferred result  $\tilde{x}$  for the outcome  $x$ , given the amplification  $e^{gt}$ ). The equivalence with  $P_B(x)$  is shown in Figure 9, for  $\alpha_0 = 2$ .

From Figure 10, we see that the trajectories for  $p$  for the cat state when  $\hat{x}$  is measured are attenuated.

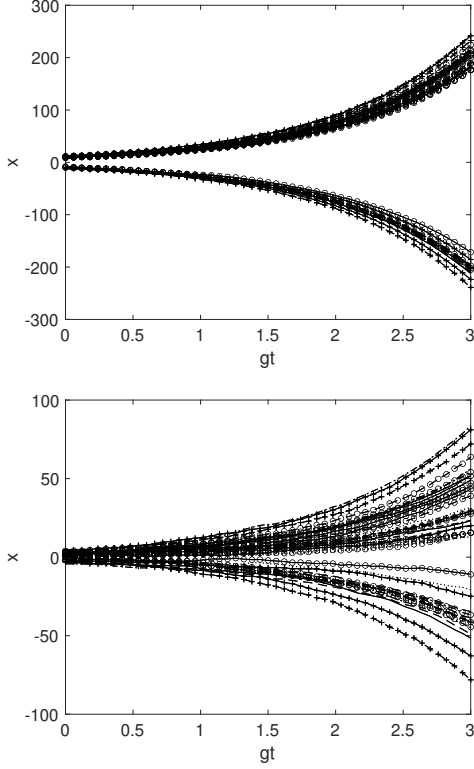


Figure 8. Measurement of  $\hat{x}$  on a cat state. Plot of backward propagating trajectories for the amplified variable  $x$  versus time  $t$  in units of  $g$ , for the system prepared in  $|cat\rangle$  (Eq. (5.11)), where  $r = 0$ . The plots show that the noise  $\langle(\Delta\hat{x})^2\rangle = 1$  associated with a coherent state is amplified. The top plot shows  $x_1 = 10$  where the coherent states are well separated. The second plot shows  $x_1 = 2$ . Here, the additional noise  $\sigma_x^2 = 1$  associated with the  $Q$  function ensures that the two peaks in the  $Q$  function associated with the two coherent states overlap at  $t = 0$ , but there is no overlap in the amplified distribution at time  $t_f$ . Here  $t_f = 3/g$ .

The effect is less pronounced when compared to that of the superposition of position eigenstates (Figure 6), because there is a reduced noise in  $p$  at the initial time. The measurement of  $\hat{x}$  as given by  $H_A$  amplifies  $\hat{x}$  and squeezes  $\hat{p}$ . The noise levels for the initial cat state are approximately at the vacuum level  $\langle(\Delta\hat{p})^2\rangle \sim 1$ , and the measurement Hamiltonian has the effect of squeezing the fluctuations in  $\hat{p}$ , as shown by the plot of the variance in  $p$  in Figure 10.

### F. Measurement of $\hat{p}$

We have analyzed measurement of  $\hat{x}$  on the superposition of two eigenstates of  $\hat{x}$ . We now consider the complementary measurement,  $\hat{p}$ . This is incompatible with an  $\hat{x}$  measurement because it requires a different meter setting, which leads to a different measurement Hamiltonian. The resulting outputs have the complementary

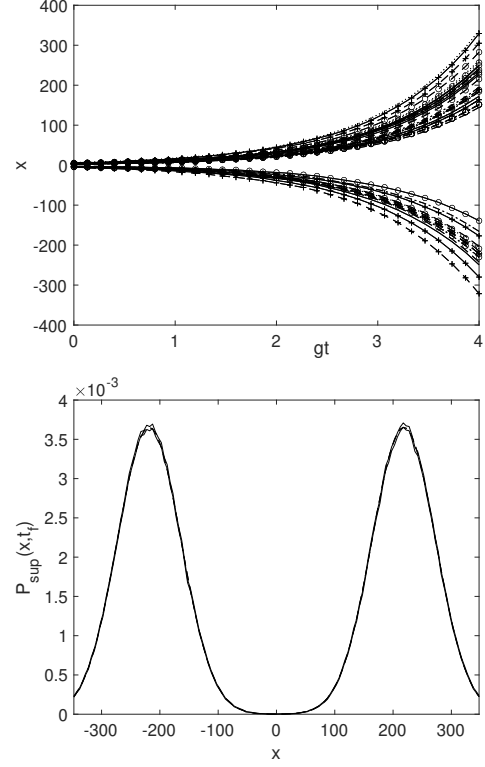


Figure 9. Measurement of  $\hat{x}$  on a cat state. Plot of backward propagating trajectories for the amplified variable  $x$  versus time  $t$  in units of  $g$ , for the system prepared in an  $r = 0$  cat state  $|cat\rangle$  (Eq. (5.11)) with  $x_1 = 4$  corresponding to  $\alpha_0 = 2$ . Also plotted is the distribution for  $P_{sup}(x, t_f)$  after the amplification. This plot agrees with the distribution  $P_B(x) = |\langle x | cat \rangle|^2$  predicted by quantum mechanics for the cat state. Here,  $t_f = 4/g$ .

feature of interference fringes.

The  $\hat{p}$  measurement requires amplification of  $p$ , with a negative  $g$  in the Hamiltonian  $H_A$ . We use

$$H_A = \frac{i\hbar g}{2} [\hat{a}^{\dagger 2} - \hat{a}^2], \quad (5.13)$$

where  $g$  is real and  $g < 0$ . The dynamics from the standard operator Heisenberg equations gives the solutions

$$\begin{aligned} \hat{x}(t) &= \hat{x}(0) e^{-|g|t} \\ \hat{p}(t) &= \hat{p}(0) e^{|g|t}, \end{aligned} \quad (5.14)$$

and we see that  $\hat{p}$  is amplified. The solutions for the dynamics of the  $x$  and  $p$  variables of the  $Q$  function are as above, except that  $x$  and  $p$  exchange roles. The trajectories for  $p$  are amplified and propagate back in time. Those for  $x$  are attenuated and propagate forward in time (Figure 11).

If we measure  $\hat{p}$  by amplifying the  $\hat{p}$  quadrature so that  $g < 0$ , then the full state at the later time is evaluated

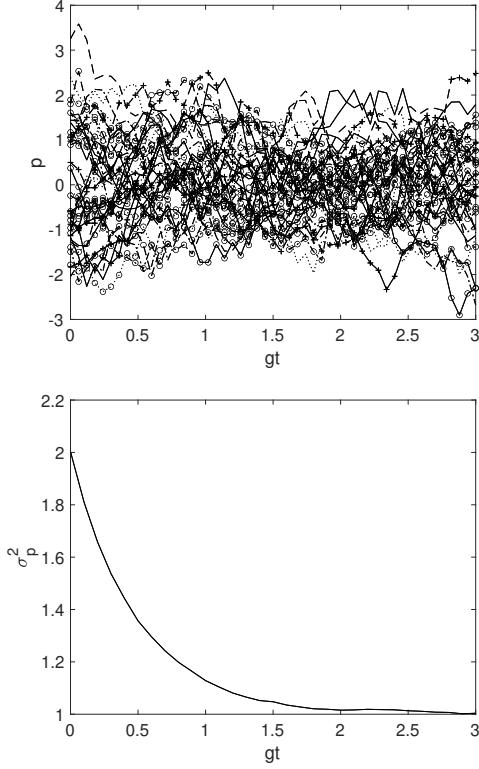


Figure 10. Measurement of  $\hat{x}$  on a cat state. Plot of forward propagating trajectories for the attenuated variable  $p$  versus time  $gt$ , for the system prepared in a cat state  $|cat\rangle$  (Eq. (5.11)). The top plot shows  $x_1 = 10$  where the coherent states are well separated. Here,  $t_f = 3/g$ . The lower plot shows the variance  $\sigma_p^2$  evaluated at each time  $gt$ , evaluated over a large sample of trajectories. The final variance  $\sigma_p^2(t)$  decays to 1.

directly as before. From (5.7), we find

$$Q_{sup}(x, p, t) = \frac{e^{-p^2/2\sigma_p^2(t)}}{4\pi\sigma_x(t)\sigma_p(t)} \left\{ e^{-(x-G(t)x_1)^2/2\sigma_x^2(t)} + e^{-(x+G(t)x_1)^2/2\sigma_x^2(t)} - 2e^{-(x^2+G^2(t)x_1^2)/2\sigma_x^2(t)} \sin\left(\frac{pG(t)x_1}{\sigma_x^2(t)}\right) \right\}, \quad (5.15)$$

where  $G(t) = e^{gt}$  and  $\sigma_{x/p}^2(t) = 2(1 \pm \tanh(r - gt))^{-1} = 1 + e^{\pm 2(gt-r)}$ , except that now  $g < 0$ . Therefore  $G(t) = e^{-|g|t} \rightarrow 0$  and  $\sigma_x^2(t) = 1 + e^{-2(|g|t+r)} \rightarrow 1$ , in the limit of  $|g|t \rightarrow \infty$ . Hence, the future marginal in  $p$  at time  $t_f$  is

$$P_{sup}(p, t) = \frac{e^{-p^2/2\sigma_p^2(t)}}{\sqrt{2\pi}\sigma_p} \left\{ 1 - e^{-\frac{G^2(t)x_1^2}{2\sigma_x^2(t)}} \sin\left(\frac{pG(t)x_1}{\sigma_x^2(t)}\right) \right\} \rightarrow \frac{e^{-p^2/2\sigma_p^2(t)}}{\sqrt{2\pi}\sigma_p} \left\{ 1 - \sin(pG(t)x_1) \right\}. \quad (5.16)$$

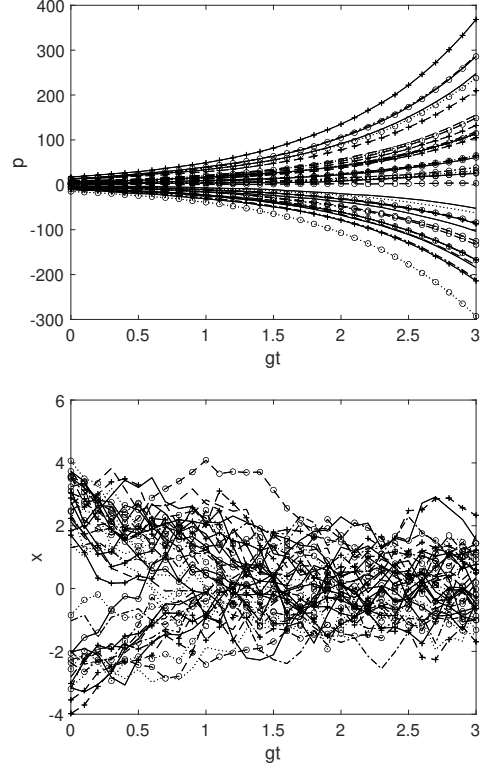


Figure 11. Measurement of  $\hat{p}$  for a system prepared at time  $t_0$  in a superposition  $|\psi_{sup}\rangle$  of two eigenstates  $|x_1\rangle$  and  $|x_2\rangle$  with  $x_1 = -x_2 = 3$ , modeled as (3.16) with  $r = 2$ . The top plot shows trajectories for  $p$  propagating according to  $H_A$  with  $g < 0$ . The final values of  $p$  at  $t_f$  are amplified. The trajectories for  $p$  propagate backwards, from the future boundary at  $t_f$ , subject to noise with variance  $\sigma_p^2 = 1$ . The lower plot shows forward propagating trajectories for the complementary variable  $x$ , which are attenuated to the vacuum noise level  $\sigma_x^2 = 1$ .

We may write the solution as

$$P_{sup}(\tilde{p}, t) \rightarrow \frac{e^{-\tilde{p}^2/(2e^{2r})}}{\sqrt{2\pi}} \left\{ 1 - \sin(\tilde{p}x_1) \right\}, \quad (5.17)$$

using the scaled variable  $\tilde{p} = p/e^{|g|t} = p/\sigma_p(t)$  and noting that  $\sigma_p(t) = e^{|g|t}e^{2r}$  for large  $|gt|$ , with  $g < 0$ .

We compare with the quantum prediction for the distribution  $P_B(p)$  for the outcome  $p$  upon measurement of  $\hat{P}$ , given as  $P_B(p) = |\langle p|\psi_{sup}\rangle|^2$ , where  $|p\rangle$  is the eigenstate of  $\hat{p}$ . We first compare for the cat state (5.11) with a real amplitude  $\alpha_0$ , where  $r = 0$ . In fact, the solution [102]

$$P_B(\tilde{p}) = \frac{e^{-\tilde{p}^2/2}}{\sqrt{2\pi}} \left\{ 1 - \sin(2\alpha_0\tilde{p}) \right\} \quad (5.18)$$

is in agreement with (5.17) (after accounting for the amplification  $e^{|g|t}$ ), upon noting that with the choice of quadrature scaling,  $x_1 = 2\alpha_0$ . Figure 12 shows the future marginal and the trajectories for  $p$ , for large  $|gt|$ . As expected, the fringes are prominent.



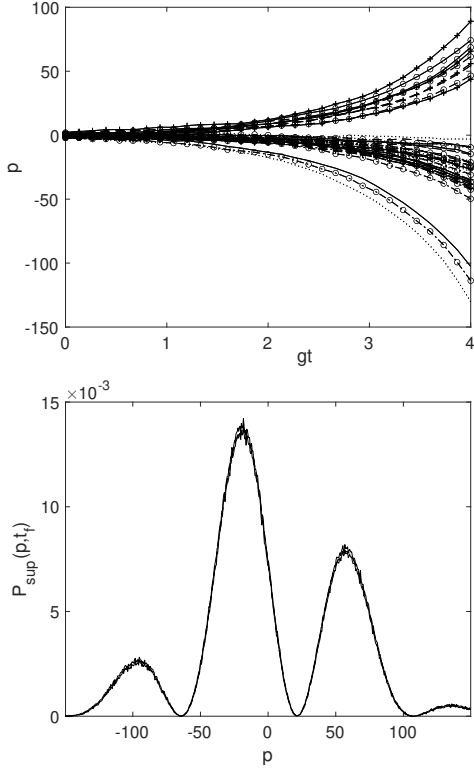


Figure 12. Plotted are the backward trajectories for  $p$  for the measurement of  $\hat{p}$ , using the Hamiltonian  $H_A$  where  $g < 0$ . We consider the cat state  $|cat\rangle$  given by Eq. (5.11) where  $r = 0$ , with well separated coherent states given by  $x_1 = 4$ . This corresponds to  $\alpha_0 = 2$ . Here,  $t_f = 4/g$ . The final distribution  $P_{sup}(p, t_f)$  is given in the lower plot. The fringes are sharply defined in agreement with  $P_B(p)$  as predicted by quantum mechanics. Graphs show the upper and lower ( $\pm\sigma$ ) sampling error values, and the exact result.

The comparison is done for the superposition  $|\psi_{sup}\rangle$  of two eigenstates in Figure 11, giving exact agreement with the standard quantum prediction. The Figure also shows the forward trajectories in the complementary variable  $x$ .

### G. Born's rule for measurements $\hat{x}$ and $\hat{p}$

As the amplification  $G$  increases to a macroscopic level, the probability distribution evaluated by sampling over the trajectories for  $x$  becomes that of  $P_B(x)$ , given by quantum mechanics. Here,  $P_B(x) = |\langle x|\psi\rangle|^2$  gives the Born rule for detecting the value  $x$  on measurement of  $\hat{x}$  for the system prepared in the state  $|\psi\rangle$ . This mechanism was explained in Section III and is evident in the Figures which display the probability for the relative outcomes  $x_1$  or  $-x_1$  for the simple superposition (3.16).

The amplified marginal distribution is

$$P_{sup}(x, t) = \frac{1}{2\sqrt{2\pi}\sigma_x(t)} \left\{ |c_1|^2 e^{-(x-G(t)x_1)^2/2\sigma_x^2(t)} + |c_2|^2 e^{-(x+G(t)x_1)^2/2\sigma_x^2(t)} \right\}, \quad (5.19)$$

where  $G = e^{gt}$  ( $g > 0$ ) and  $\sigma_x^2(t) = 1 + e^{2gt-2r}$ . Defining the scaled variable  $\tilde{x} = x/e^{gt}$ , this becomes

$$P_{sc}(\tilde{x}, t) = \frac{1}{2\sqrt{2\pi}\sigma_{\tilde{x}}(t)} \left\{ |c_1|^2 e^{-(\tilde{x}-x_1)^2/2(e^{-2gt}+e^{-2r})} + |c_2|^2 e^{-(\tilde{x}+x_1)^2/2(e^{-2gt}+e^{-2r})} \right\}. \quad (5.20)$$

On taking  $gt$  large, this gives

$$P_{sc}(\tilde{x}, t) = \frac{1}{2\sqrt{2\pi}} \left\{ |c_1|^2 e^{-(\tilde{x}-x_1)^2/(2e^{-2r})} + |c_2|^2 e^{-(\tilde{x}+x_1)^2/(2e^{-2r})} \right\}. \quad (5.21)$$

The eigenstates of  $\hat{x}$  correspond to  $r \rightarrow \infty$  where the Gaussian peaks become infinitely narrow. The value of  $x_1$  which corresponds to the separation between the peaks is much larger than the width of the Gaussian distributions. Hence, the relative probability for observing  $x_1$  or  $-x_1$  is given by the relative weighting of the peaks,  $|c_1|^2$  and  $|c_2|^2$ , in accordance with Born's rule for the measurement postulate. The amplified, scaled marginal becomes  $P_B(x)$  because in this limit of large amplification the vacuum noise term given by 1 in the expression (3.18) for  $\sigma_x^2$  is *not* amplified, whereas  $x_1$  and any extra noise above 1 is amplified. The analysis can be extended for an arbitrary expansion  $|\psi\rangle = \sum_i c_i |x_i\rangle$  where  $|x_i\rangle$  are eigenstates of  $\hat{x}$ , to validate Born's rule for  $\hat{x}$ . The example of validation of  $P_B(x) = |\langle x|\psi_{sup}\rangle|^2$  where there is a continuum of states  $|x_i\rangle$  is given by the example of the cat state, in Figure 9.

We similarly demonstrate Born's rule for measurement  $\hat{p}$ . We expand in eigenstates  $|p\rangle$  of  $\hat{p}$  as  $|\psi_{sup}\rangle_p = \sum_j d_j |p_j\rangle$ , where  $d_j$  are probability amplitudes. Using the overlap function

$$\langle p_j|\alpha\rangle = \frac{1}{\pi^{1/4}} \exp\left(-\frac{(p-p_j)^2}{4} - \frac{i}{2}x(p_j-2p)\right), \quad (5.22)$$

the  $Q$  function for this state is then given by

$$Q(x, p) = \frac{1}{\pi^{3/2}} \left| \sum_j d_j e^{-\frac{1}{4}(p-p_j)^2} e^{-i\frac{x}{2}(p_j-2p)} \right|^2. \quad (5.23)$$

This is a sum of Gaussians combined with interference cross-terms. Following the analysis of Section III for  $\hat{x}$ , we see that on amplification of  $\hat{p}$  the final distribution  $Q(x, p, t_f)$  will become a set of narrow Gaussians in  $p$  centered at  $p_j$  with weighting  $|d_j|^2$ . The interference terms vanish in the limit of large amplification. The realization of Born's rule for  $\hat{p}$  is evident in the examples of Section V.F, shown in Figure (12).

## VI. CONNECTING $x$ AND $p$ TRAJECTORIES: CAUSAL LOOPS

How do the trajectories for the superposition  $|\psi_{sup}\rangle$  differ from those of the mixture  $\rho_{mix}$  of eigenstates  $|x_j\rangle$ ? We examine the coupling between the  $x$  and  $p$  trajectories, where one measures  $\hat{x}$ .

At time  $t = t_0 = 0$ , the  $Q$  function (3.13) (and (3.19)) for the superposition  $|\psi_{sup}\rangle$  shows a correlation between  $x$  and  $p$ . This is not the case for the mixture  $\rho_{mix}$  (3.14), the  $Q$  function for the single eigenstate  $|x_1\rangle$  factorizing with respect to  $x$  and  $p$ . The  $x$  and  $p$  trajectories for the superposition (but not for a mixture  $\rho_{mix}$ ) are therefore correlated i.e. connected (Figure 4).

### A. Conditional distribution at the boundary

We see that a given  $x_f$  from the future time  $t_f$  propagates for each trajectory to a single  $x_p$  in the present time, at  $t_0$ . For each  $x_p$ , there is a set of  $p_p$  at the present time. This set is given by the conditional distribution  $P_Q(p_p|x_p) = Q(x_p, p_p, 0)/P(x_p)$  evaluated from the  $Q$  function in the present, where  $t = t_0 = 0$ . Here,  $P(x_p)$  is the marginal (5.9) at time  $t_0$ :  $P(x_p) \equiv P(x_p, 0)$ . Evaluating for the superposition  $|\psi_{sup}(r)\rangle$ , we find

$$P_Q(p_p|x_p) = P(x, p, 0)/P(x, 0) = \frac{e^{-p_p^2/2\sigma_p^2}}{\sigma_p\sqrt{2\pi}} \left\{ 1 - \frac{\sin(p_p x_1/\sigma_x^2)}{\cosh(x_p x_1/\sigma_x^2)} \right\}, \quad (6.1)$$

which becomes  $\sim 1 - \sin(p_p x_1) \text{sech}(x_p x_1)$  for  $r$  large. Fringes are evident, these becoming finer for large  $x_1$ , and also increasingly damped, provided  $x_p \neq 0$ . For smaller  $x_1$ , the fringes will be more prominent, regardless of  $G$ . The conditional distribution implies that the trajectories for  $x$  and  $p$  are coupled i.e. correlated. For a set of values of  $x_f$  at the time  $t_f$ , we can match the set with a set of  $p$  trajectories, by propagating each given  $p_p$  from the sample generated by  $P(p_p|x_p)$ , back to the future  $t_f$ . We then have sets of variables  $\{x_f, x_p, p_p, p_f\}$  and all intermediate values on the trajectories. Such sets of trajectories are plotted in Figure 13.

The coupling of the  $p$  trajectories with those for  $x$  is determined by  $P_Q(p_p|x_p)$ . We ask how does this depend on which state  $|x_1\rangle$  or  $|-x_1\rangle$  the system is measured to be in? The function  $P_Q(p_p|x_p)$  is *independent* of the sign of  $x_p$  and hence is not sensitive to which state the system is measured to be in. This is evident in Figure 13 which plots the distribution for the trajectories of  $p$  conditioned on a positive final outcome i.e.  $x_f > 0$ . Considering the the causal relations depicted in Figure 4, this implies that the conditional relation giving  $p$  from  $\delta x$  is not dependent on  $\lambda = x_j$ .

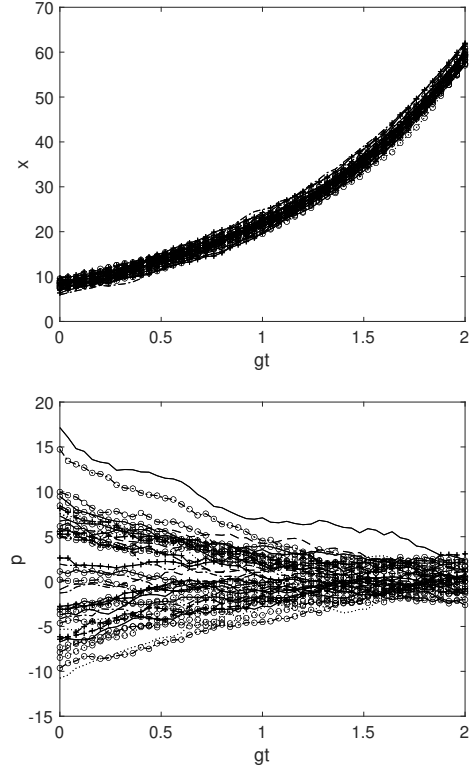


Figure 13. Plots show trajectories for  $x$  and  $p$  for the system prepared in a superposition  $|\psi_{sup}\rangle$ , conditioned on a positive outcome for measurement of  $\hat{x}$ . Here, we take  $|\psi_{sup}(r)\rangle$  of (3.16) with  $r = 2$ ,  $x_1 = 8$  and  $t_f = 2/g$ .

It is important to also note that the conditional distribution  $P_Q(p_p|x_p)$  for the mixture  $\rho_{mix}$  of the two eigenstates is given by

$$P_Q(p_p|x_p) = \frac{e^{-p_p^2/2\sigma_p^2}}{\sigma_p\sqrt{2\pi}}, \quad (6.2)$$

which implies *complete independence* of the trajectories for  $x$  and  $p$ . The coupling of these trajectories at the boundary  $t = t_0$  distinguishes a superposition  $|\psi_{sup}\rangle$  from a mixture  $\rho_{mix}$ . The trajectories for  $x$  follow directly from the marginals  $P(x, t_f)$  in each case, and are hence identical (since the  $P(x, t_f)$  are identical). This tells us that the causal loop is the feature distinguishing the superposition (and hence ultimately entanglement) from the mixed state.

Next, we ask what happens if we postselect on the condition that the final outcome of the measurement  $\hat{x}$  is  $x_1$ : that is,  $x_f > 0$ ? We evaluate the sets  $\{x_f, x_p, p_p, p_f\}$  conditioned on  $x_f > 0$ , for large amplification  $G$ , which corresponds to a measurement. In Figure 13, we depict such sets for  $x_f > 0$ , and the forward trajectories in  $p$  for the set  $x_f > 0$ , and also the related distribution  $P_+(p)$  for the forward trajectories at the given times  $t$ . We ask what can we say about the state at the initial time  $t_0$  i.e. in the present, given this postselection?

### B. Inferred initial state for $x$ and $p$ postselected on a measurement outcome $x_j$

We bin the final outcomes into positive and negative  $x_f$ , which would allow the final observer to infer either  $x_1$  or  $-x_1$  as the “result of the measurement”, in the limit of large amplification  $gt$ . In our reality model, one can calculate the “state” of the original distribution (at  $t = t_0$ ) corresponding to connected trajectories in  $x$  and  $p$ , conditioned on the positive outcome  $x_1$ .

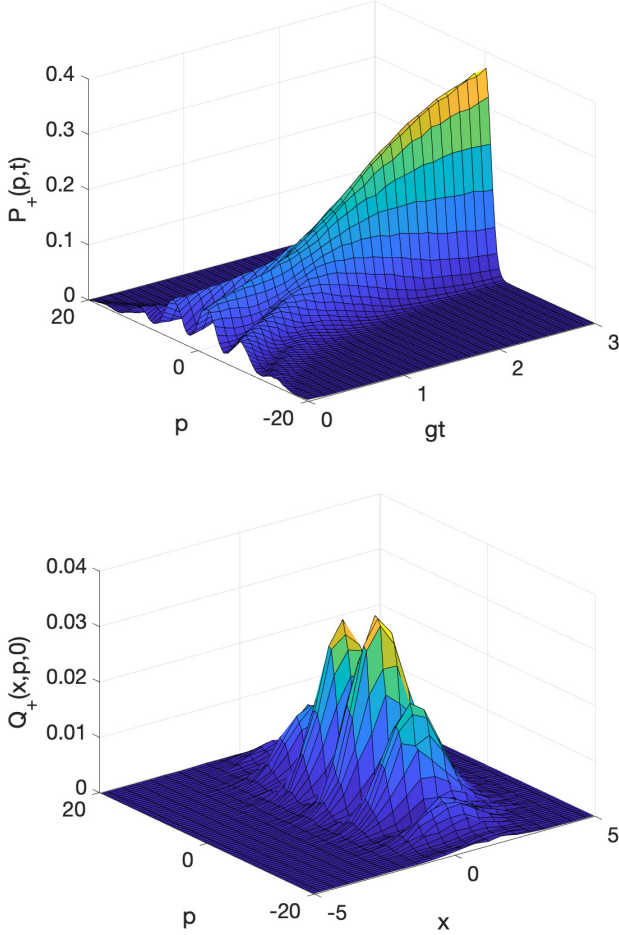


Figure 14. Measurement of  $\hat{x}$ . The upper plot shows the distribution for  $p$  versus  $gt$  conditioned on the positive outcome of measurement, for  $x_1 = 1$  and  $t_f = 3/g$ . Despite the conditioning on a positive outcome for  $\hat{x}$ , the lower plot is indistinguishable from Figure 7. The lower plot is the distribution  $Q_+(x, p, 0)$  for the inferred state at time  $t_0 = 0$ , postselected on the positive outcome  $x_1$  for  $\hat{x}$ , that is,  $x_f > 0$  at  $t_f$ , for the system prepared in the superposition  $|\psi_{sup}\rangle$  of two  $\hat{x}$  eigenstates. In practice we take  $|\psi_{sup}(r)\rangle$  (Eq. (3.16)) with  $r = 2$ .

We evaluate the joint distribution  $Q_+(x, p, t_0)$  at  $t = t_0 = 0$  corresponding to the sets of connected trajectories for  $x$  and  $p$ , based on the post-selected positive outcome  $+x_1$  for the measurement  $\hat{x}$ . As explained in

the last section, these are evaluated by way of the conditional  $P_Q(p|x)$  at time  $t = t_0 = 0$ . The distribution  $Q_+(x, p, 0)$  has the interpretation in some realism-models (e.g. the OFR model, refer to Section VIII) as describing the “state” inferred at time  $t_0 = 0$ , given the positive outcome  $x_1$  for  $\hat{x}$ . Here, we evaluate the variances  $\sigma_{x,+}^2$  and  $\sigma_{p,+}^2$  of the inferred distribution  $Q_+(x, p, 0)$ , and show that they correspond to variances below the level allowed by the Heisenberg uncertainty principle.

We proceed as follows. For sufficiently large  $gt$ , each  $x_f$  is either positive or negative, associated with the outcome  $x_1$  or  $-x_1$  which we denote by  $+$  or  $-$ . We trace the trajectories in  $x$  back to the time  $t_0 = 0$  given the post-selection of  $x_f > 0$ , and construct the distribution of  $x$  at time  $t_0 = 0$  for all such trajectories, as explained in the last sections. At the boundary in the present time  $t_0 = 0$ , each value of  $x$  is connected to a set of trajectories in  $p$ , according to the conditional distribution (6.1). We thus construct the joint distribution  $Q_+(x, p, 0)$  describing the correlated values in  $x$  and  $p$  at the time  $t_0 = 0$  (Figure 14). We then determine the variances  $\sigma_{x,+}^2 \equiv \sigma_{x,+}^2(0)$  and  $\sigma_{p,+}^2 \equiv \sigma_{p,+}^2(0)$  for  $x$  and  $p$  for this distribution, and define the associated observed variance for the present  $x_p$  and  $p_p$  once antinormal ordering is accounted for:

$$\begin{aligned} [\Delta(x_p|+)]^2 &= \sigma_{x,+}^2(0) - 1 \\ [\Delta(p_p|+)]^2 &= \sigma_{p,+}^2(0) - 1. \end{aligned} \quad (6.3)$$

Similar variances  $\sigma_{x,-}^2(0)$ ,  $\sigma_{p,-}^2(0)$ ,  $[\Delta(x_p|-)]^2$  and  $[\Delta(x_p|-)]^2$  could be determined for the trajectories post-selected on the  $x_f < 0$  corresponding to the outcome  $-x_1$ . This tells us what we infer about the original state (in the reality model) at time  $t = 0$  based on the measurement outcome, whether  $+$  or  $-$ . Here, by subtracting the vacuum term 1 associated with the antinormal ordering operators, we evaluate the variances that would be associated with a measurement of  $\hat{x}$ .

The variances are given in Figure 15 versus  $x_1$  (which gives the separation between the states of the superposition) for a large value of  $gt$ . We also define the uncertainty product for the inferred initial state:

$$\epsilon = \Delta(x_p|+)\Delta(p_p|+). \quad (6.4)$$

From the Figures 15, see that  $\epsilon < 1$  for all  $\alpha$ , although  $\epsilon \rightarrow 1$  as  $x_1 \rightarrow \infty$ .

The figures show what happens if we postselect on the positive outcome,  $x_1$ , for a measurement of  $\hat{x}$ . This result is highly sensitive to the initial separation (given by  $x_1$ ) of the eigenstates, or of the coherent states  $|\alpha_0\rangle$  and  $|- \alpha_0\rangle$ . For the cat state where  $r = 0$  and  $x_1 = 2\alpha_0$  is large, the  $x$ -variance  $[\Delta(x_p|+)]^2$  is reduced almost to the vacuum level of 1, as would be expected. This is explained as follows. The overall variance in  $x$  at the time  $t_p = 0$  is large, due to there being two states comprising the superposition, but the final amplified outcome of either  $x_1 = 2\alpha_0$  or  $-x_1 = -2\alpha_0$  (Figure 9) links the trajectory back to only *one* of these states,  $|\alpha_0\rangle$  or  $|- \alpha_0\rangle$ , which have a variance in  $x$  of 1.

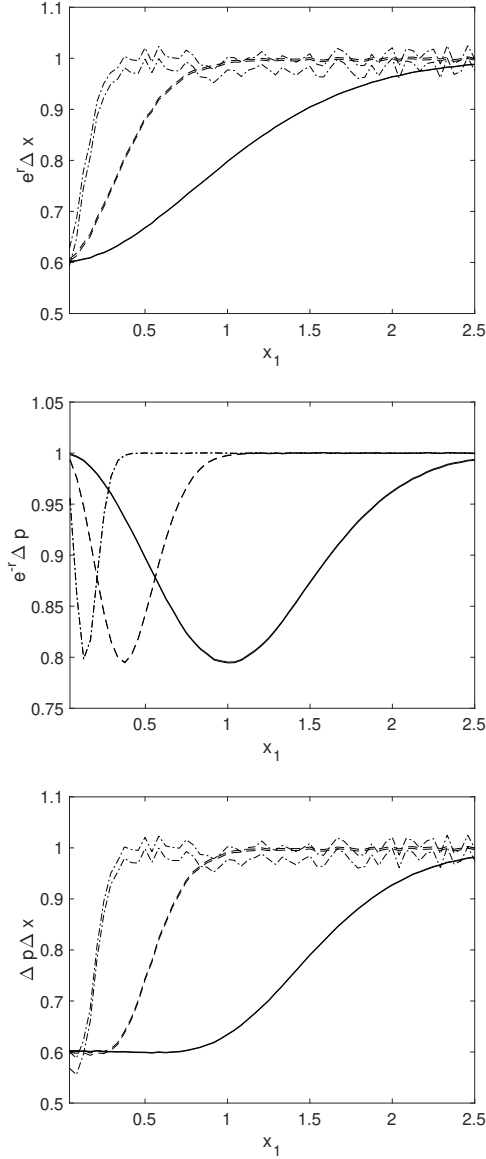


Figure 15. Inferred state at time  $t_0$  given the positive outcome for  $\hat{x}$ , i.e.  $x_f > 0$ . Here we plot the variances  $\Delta(x_p|x_f > 0)$ ,  $\Delta(p_p|x_f > 0)$  and the uncertainty product  $\epsilon = \Delta(x_p|x_f > 0)\Delta(p_p|x_f > 0)$  conditioned on a positive outcome  $x_1$  for  $\hat{x}$ , using Eq. (3.16). The upper dashed-dotted line is for a superposition  $|\psi_{sup}\rangle$  of two eigenstates of  $\hat{x}$  with  $r = 2$ , and  $x_1 = 1$ . The dashed line is for  $|\psi_{sup}(r)\rangle$  with  $r = 1$ . The solid line is for  $r = 0$ . In each case,  $gt = 4$ , which corresponds to an effective measurement of  $\hat{x}$ . The two parallel lines indicate the upper and lower error bounds from sampling errors, with  $1.2 \times 10^7$  trajectories.

A further reduction for the variance in  $x_p$  is observed because of the truncation that occurs with the Gaussian function at  $t_f$ . The conditioning is done for  $x_f > 0$ , which does not take account of the negative values in  $x_f$  associated with the Gaussian centered at  $x_f = gx_1$ . This effect becomes negligible for a superposition of true eigenstates

of  $\hat{x}$  ( $r \rightarrow \infty$ ) in the limit of a true measurement corresponding to  $gt \rightarrow \infty$ , as observed when comparing the results of Figure 15. However, the variance  $[\Delta(p_p|+)]^2$  in  $p$  occurs from the distribution for  $p$  that has interference fringes. This is more pronounced with smaller separation  $x_1$ . The fringe pattern leads to a reduction in the variance, as compared to the simple Gaussian in  $p$  [112, 113]. This effect is stable for  $gt$  and  $r$ , although at greater  $r$  we see that the optimal dip in the variance occurs at smaller separations  $x_1$  of eigenstates.

The overall result is that the Heisenberg uncertainty principle is not satisfied for the coupled  $x$  and  $p$  trajectories: i.e., the post-selected  $Q$  function distribution  $Q_+(x, p, 0)$  does not reflect a “true” quantum state  $\psi$  in the standard sense. Due to the fringes becoming finer as  $x_1 \rightarrow \infty$ , the product approaches 1 with increasing separation of the eigenstates. This reveals that the variables  $x_p$  and  $p_p$  that we may identify as “elements of reality” are *inconsistent* with a standard quantum state, but become so in the limit of large  $x_1$ , where one has a true macroscopic superposition – a “cat state”.

## VII. CAUSAL RELATIONS

A question might be “*by how much can noise from the future boundary affect the present reality*”? For measurements on a macroscopic superposition  $|\psi_{sup}\rangle$  of eigenstates  $|x_j\rangle$ , where the separation of between the eigenvalues  $x_j$  is well beyond 1 (in units where  $\hbar = 1$ ), the answer would be zero (refer to Figure 1). However, microscopic differences for the trajectories are apparent.

### A. Causal structure

We examine the phase-space simulations of the measurement on the superposition  $|\psi_{sup}\rangle$  (Eqs. (2.1) and (3.12)). The simulations involve classical-like amplitudes, and hence we can identify a causal model associated with the procedure of the simulation. For example, if a hidden variable  $\lambda_M$  can be assigned to the state at time  $t = 0$  and this determines the outcome  $x_1$  or  $-x_1$  for  $\hat{x}$ , we argue that there is a causal relation. This is postulated by some models of realism eg. the weak realism (wR) (for all  $x_1$ , subject to the measurement setting) and macroscopic-realism (MR) models (for  $x_1$  large), as explained in the next section. However, the sampling from the future boundary at  $t = t_f$  ensures a type of retrocausality, at the level of the quantum vacuum noise.

The causal relations for the simulation are depicted in Figure 16. We select the simplest relations. We denote the measurement by  $\hat{X}$ , where  $\hat{X}$  is either  $\hat{x}$  or  $\hat{p}$ . The model parameters are the measurement setting  $\theta$  (in this case, the choice to measure either  $\hat{x}$  or  $\hat{p}$ ) and the variables that describe the state of the system, at the times  $t = t_0 = 0$ , and  $t = t_f$ , as well as the noise inputs  $\xi_1(t)$

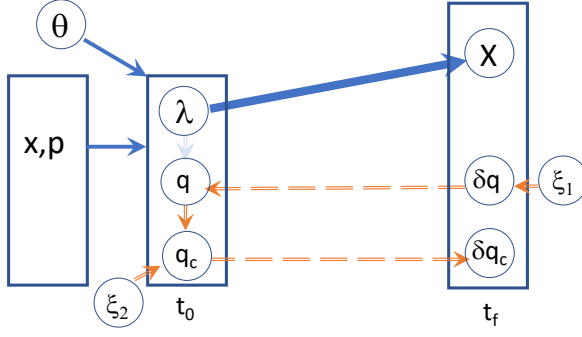


Figure 16. Macro-micro causal relations for the simulation given by the trajectories shown in the Figures of this paper, e.g. Figures 1, 4 and 12. The joint probability for  $x$  and  $p$  is given by  $Q(x, p)$ . The  $\theta$  is the measurement setting, determining whether  $\hat{x}$  or  $\hat{p}$  is measured, and  $\lambda$  is an eigenvalue  $x_j$  (or  $p_j$ ) of  $\hat{x}$  (or  $\hat{p}$ ) depending on the setting  $\theta$ .  $X$  is the amplified system variable at the time  $t_f$  which corresponds to the outcome of measurement in the simulation. The relation between  $\lambda$  and  $X$  is deterministic,  $X$  being a direct amplification of the eigenvalue. Here,  $\delta q$  represents the (unmeasured) fluctuation at time  $t_f$ , which is linked back to the measured variable ( $x$  or  $p$ ) at time  $t_0$ . If, for instance,  $\theta$  corresponds to  $\hat{x}$ , the conditional distribution  $P_Q(p|x)$  at  $t = t_0 = 0$  given by (6.1) determines the conditional relation between  $q \equiv x$  and  $q_c \equiv p$ , which is the correlation specified by  $x, p$  at time  $t_0$ . That relation then determines the relation for the (unmeasured) fluctuation  $\delta q_c$  at time  $t_f$ .

and  $\xi_2(t)$ . Where we measure  $\hat{x}$ , the notation implies  $\xi_1(t) \equiv \xi_x(t)$  and  $\xi_2(t) \equiv \xi_p(t)$ .

The  $Q$  function specifies the system variables at time  $t_0$  (or just prior) to be  $x$  and  $p$ , with joint probability  $Q(x, p, t_0)$ . To proceed with the simulation, the backward trajectories originate from the *future marginal* that represents the amplified state. This marginal is subject to the choice of measurement setting  $\theta$ , and can in principle be derived from the dynamical equation for the  $Q$  function. As we have seen, the solutions show that the future marginal (and hence the boundary condition) is identical to that of the mixture of eigenstates of  $\hat{X}$ , for which the system is probabilistically in a state with a definite outcome for the measurement  $\hat{X}$ , the outcomes being one of the eigenvalues  $\lambda$ . The procedure of sampling for the *backward* trajectories is hence identical to that used for the mixed state: Each individual trajectory (or run) is specified by a value of  $\lambda$ , the value being one of the set of eigenvalues  $\{x_j\}$  (or  $\{p_j\}$ ) of the measurement  $\hat{x}$  (or  $\hat{p}$ ). The relative weighting for  $\lambda$  in the simulations is determined by the future marginal, and is given by the probability amplitudes consistent with Born's rule. We define the conditional

$$P(\lambda|\theta), \quad (7.1)$$

where  $P(\lambda = x_j) = |c_j|^2$  if  $\theta \equiv \hat{x}$  and  $P(\lambda = p_j) = |d_j|^2$  if  $\theta \equiv \hat{p}$ . Here,  $|c_j|$  and  $|d_j|$  are determined by the

$Q$  function  $Q(x, p)$ , from the marginals  $P(x)$  (or  $P(p)$ ) found by integrating over the complementary variable ( $p$  or  $x$ ), but are given quantum mechanically by  $c_j = \langle x|\psi \rangle$  and  $d_j = \langle p|\psi \rangle$ . Here,  $|\psi \rangle$  is the quantum state at time  $t_0$ . We do *not* define an underlying joint distribution  $P(\lambda_x, \lambda_p)$  for variables that correspond to  $\lambda = \lambda_x$  if  $\theta \equiv \hat{x}$ , and  $\lambda = \lambda_p$  if  $\hat{p}$ . The causal diagram corresponds to the weak-realism model described in Section VIII. For a macroscopic superposition, the diagram corresponds to the macroscopic-realism model.

The final measured outcome value will be  $X$ , which is the *amplified value* of  $\lambda$ . In the model,  $X$  is also a system variable at the time  $t_f$ . The relation between  $X$  and  $\lambda$  (and  $\theta$ ) is deterministic, ie.

$$X = e^{|g|t} \lambda, \quad (7.2)$$

where  $\lambda = x_j$  for some  $j$ , if  $\theta \equiv \hat{x}$ ; and  $\lambda = p_j$  for some  $j$ , if  $\theta \equiv \hat{p}$ . This causal deterministic relation is represented by the blue forward-going solid arrow in Figure 16. With the choice of  $\theta$ , there is a value  $\lambda$  selected, with a certain probability. This may be regarded as a macroscopic causal relation (and for macroscopic superpositions, where  $\lambda$  is macroscopic) since it relates to a measured quantity.

The system at time  $t_f$  includes the fluctuations  $\delta q$  that are not measured by amplification, where  $q$  is either  $x$  or  $p$ . The value of  $\delta q$  is then sampled using a random Gaussian function  $P_G$  with mean 0 and variance  $\sigma_x^2 = 1$  at time  $t_f$ . Hence

$$P(\delta q(t_f)) \equiv P_G(0, \sigma_x). \quad (7.3)$$

The value of the system variable  $q$  is  $q = q_j + \delta q(t_f)$ , and  $q_j$  is either  $x_j e^{|g|t_f}$  or  $p_j e^{|g|t_f}$ , depending on the value of  $\theta$ . The backward trajectory is given by

$$\frac{dq}{dt_-} = -|g|q + \sqrt{2g}\xi_1(t), \quad (7.4)$$

as in (7.5), with the initial condition being the value of  $q$  at time  $t_f$ . The Gaussian random noise  $\xi_1(t)$  satisfies  $\langle \xi_1(t) \xi_1(t') \rangle = \delta(t - t')$  and decouples from the complementary variable  $q_c$  (which is either  $p$  or  $x$ ). We note however we can solve (7.5) by substituting  $q = q_0 + \delta q$ , where  $q_0$  satisfies

$$\frac{dq_0}{dt_-} = -|g|q_0 \quad (7.5)$$

with initial condition  $q_0(t_f) = q_j$ , and

$$\frac{d(\delta q)}{dt_-} = -|g|\delta q + \sqrt{2g}\xi_1(t), \quad (7.6)$$

with initial condition  $\delta q = \delta q(t_f)$ . Clearly, the solution for  $q_0$  is the deterministic function  $q_0 = q_j e^{-|g|t_-}$ , which is either  $q_0 = x_j e^{|g|(t_f - t_-)}$  or  $q_0 = p_j e^{|g|(t_f - t_-)}$  depending on the value of  $\theta$ , the measurement setting. This decaying solution with respect to  $t_-$  is evident in the trajectories for  $x$  plotted in Figures 1 and 4. The trajectory

for  $\delta q$  has a stochastic solution involving the noise  $\xi_1$ . This noise does *not* depend on the value of  $q_0$  or  $q$ , but rather has constant size. The consequence is that the  $\delta q$  has the same initial condition and trajectory equations, regardless of whether the measured quantity  $q$  is  $x$  or  $p$ .

The trajectory for  $\delta q$  propagates back to  $t_0$  with a value  $\delta q(t_0) = q_p$  (in the present time). Hence, we write

$$P(\delta q(t_0)) \equiv P(\delta q(t_0)|\delta q(t_f)), \quad (7.7)$$

noting that the noise value  $\delta q$  is *independent* of the value of  $X$  (that is,  $x_j$  or  $p_j$ ) and, perhaps surprisingly,  $\theta$ . This defines the backward retrocausal relation marked by the red dashed arrow in the Figure 16.

However,  $q$  is either  $x$  or  $p$  - which is determined at the present time  $t_0$ , from  $\theta$ . The value of the complementary variable that is *not* measured is denoted  $q_c$ . Here,  $q_c$  is either  $p$  or  $x$ . The value  $\delta q_c(t_0)$  can be specified according to the conditional  $P_Q(q_c|q)$  at time  $t_0$ . The  $\delta q(t_0)$  defines the value of  $q$  at time  $t_0$ :  $q = \lambda + \delta q(t_0)$ . This determines  $q_c$  at time  $t_0$ . Denoting the values of  $x$  and  $p$  at time  $t_0$  as  $x(t_0) = x_p$  and  $p(t_0) = p_p$  (meaning  $x$  and  $p$  in the present time), we write if  $q = x$  and  $q_c = p$  that

$$P_Q(p(t_0)|x(t_0)) = P_Q(p(t_0)|x(t_0)) \equiv P_Q(p_p|x_p), \quad (7.8)$$

and if  $q = p$  and  $q_c = x$  that

$$P_Q(x(t_0)|p(t_0)) = P_Q(x(t_0)|p(t_0)) \equiv P_Q(x_p|p_p). \quad (7.9)$$

This conditional relation is given by the short red downward arrow at the boundary  $t = t_0$  in Figure 16. The value of  $q_c(t_0)$  determines the starting point of the trajectory that results in a value  $q_c(t_f)$  for the complementary variable  $q_c$  at time  $t_f$ . The probability

$$P(q_c(t_f)|q_c(t_0)) \quad (7.10)$$

is well defined stochastically by the forward dynamics given by equation (5.5), which involves the noise function  $\xi_2$ . This relation is causal and is marked on Figure 16 by the forward arrow. The relations given by the red dashed arrows can be regarded as microscopic, or hidden, since they govern quantities that are not measured.

For the particular Hamiltonian  $H_A$ , the equations for  $x$  and  $p$  decouple, which simplifies the nature of the causal loop. The  $x$  and  $p$  variables decorrelate with time  $t_f$ , as  $t_f \rightarrow \infty$ . The loop is hence closed consistently at the future boundary. The consistency of the correlations with those of  $Q(x, p, t)$ , as solved from the Hamiltonian  $H_A$ , has been verified (Section IV.C).

## VIII. MODELS OF REALISM

The causal model presented in the previous section has a classical nature and hence suggests classical-type models of realism. We examine the level of consistency between the causal model and each of the realism-models that might be considered. The models presented *cannot*

be interpreted as a Bell local hidden variable theory. This is discussed in the companion paper [114], and is related to the boundary conditions imposed in the future in our implementation of the meter trajectories, which leads to cyclic loops.

### A. Objective field realism model

The interpretation of this model – objective field realism (OFR) – is that the physical system at any time  $t_0$  is in an *objective field state* specified by the values  $x$  and  $p$  with probability  $Q(x, p, t_0)$ . This defines an underlying reality in the sense described by Born [54]. The amplitudes  $x$  and  $p$  however cannot be directly measured. In the OFR interpretation, this is not due to any lack of reality, but is caused by the fact that the system and measuring instruments have vacuum noise, and interact with the system being measured. The  $Q$  function is a joint probability distribution for the objective fields  $x$  and  $p$ , but  $x$  and  $p$  do not directly correspond to the measurable outcomes until one adds a model for the meter itself. The microscopic values are different to the macroscopic meter outputs. The macroscopic outputs are the values recorded by the observer. Measurement has no special treatment, but it must involve a physical amplification by a meter that has a macroscopic output in order to be regarded as a measurement. This leads to contextuality, as the meter interacts with the quantum system.

The  $Q$  model is described as “retrocausal”, since the equations of motion depend on future boundary values, not just on past boundary values as in Bell’s model [8]. Our definition is similar to Dirac’s theory of radiation reaction [115]. This also has future boundary values, which Dirac described as follows: “*We now have a striking departure from the usual ideas of mechanics. We must obtain solutions of our equations of motion for which the initial position and velocity of the electron are prescribed, together with its final acceleration, instead of solutions with all the initial conditions prescribed.*”

The model is considered “objective”, in the same way that Dirac’s theory, or Wheeler-Feynman’s absorber theory, based on classical electrodynamics, is also considered an objective theory. We introduce quantum features through noise sources not present in such earlier classical theories. The simplest interpretation is that these are objective trajectories which are time-symmetric. Such an objective model, like the fundamental physical laws, has no preference for past or future. It makes no distinction between measurement or any other physical process, and, it is argued, does not need human agency to define reality. Another way to define realism is via experimental preparation and measurement. We regard such conventional definitions as an epistemological “ladder” [116] to microscopic pictures.

It is often thought that retrocausal models are fundamentally unlikely to be correct because retrocausality is not observed in everyday life, at a macroscopic level. Yet

irreversibility is known to occur even in classical statistical mechanics at a macroscopic level, despite the reversibility of Newton's laws. An argument given for the lack of observation of everyday retrocausality is that this is simply due to imperfect experimental control on the future boundary conditions [11]. Another argument is from the solutions given in this paper, which show how retrocausation may exist microscopically, while macroscopic realism and causality hold macroscopically.

### B. A deterministic-contextual model: weak realism

A different model adopts the stronger, more conventional definition of realism – that the outcome of a measurement is in some way predetermined. This form of realism must necessarily be weaker than that proposed by Bell, which can be falsified [8], and is motivated by the causal model presented in the last section.

The causal model is based on the procedural method of the simulation combined with the principle of Occam's razor, to find the consistency with macroscopic causality in the simplest way. The backward trajectories  $x(t)$  for the system prepared at time  $t = 0$  in a superposition  $|\psi_{sup}\rangle$  of eigenstates  $|x_j\rangle$  are governed by the same equations as those for the system prepared in a mixture  $\rho_{mix}$  of eigenstates, the future boundary conditions being identical. The system  $\rho_{mix}$  is in a state of definite outcome  $x_j$  at the time  $t = 0$ . Hence, the causal model is based on the assumption that at the time  $t \sim 0$  the system is in a 'state' with definite value for the outcome  $\lambda_j \equiv x_j$ . The outcome can be described by a variable  $\lambda$ : the set of  $\lambda$  is the set  $\{x_j\}$ . We refer to such a model as a *weak-realism* (wR) model, following the work of [45, 117], and Bell's suggestion of 'beables' [118]. Here, realism is linked with causality, that the future is affected by the present and past (not vice versa). The wR model does *not* imply that the system is at time  $t = 0$  in an eigenstate  $|x_j\rangle$  (indeed it cannot be), but allows a different formulation for the state. In such a model, the probability that the system is in a state giving outcome  $x_j$  is  $|c_j|^2$ . For consistency with the simulations, this model would be combined with microscopic retrocausal-causal relations.

The wR model needs qualification. In its simplest form, the model would contradict the known contextuality of quantum mechanics [119, 120]. The ket  $|\psi_{sup}\rangle$  can be written as a linear combination of eigenstates of either  $\hat{x}$  or  $\hat{p}$ . The simplest form of the model would then imply simultaneous specification (at time  $t_0$ ) of the outcomes for  $\hat{x}$  and  $\hat{p}$  and  $\hat{O}$ , which can be negated. The  $Q$  function is a distribution function of variables  $x$  and  $p$ , but this does *not* correspond to a positive joint probability for outcomes  $x = x_j$  and  $p = p_j$  at time  $t_0$ . Hence, the wR model must account for contextuality. The model specifies that the interpretation of realism can be given for the final amplified value  $Gx_j$  (or  $Gp_j$ ), but *only* in a context where the measurement setting is specified. We conclude that the predetermination of the value  $\lambda_j$  is for

the system defined at time  $t \sim 0$ , *conditioned on the measurement setting* (e.g. whether to measure  $\hat{x}$  or  $\hat{p}$ ) being established. The model is a *deterministic-contextual realism* model – deterministic because the value for the outcome is determined at  $t \sim 0$ , but only when the context of the measurement setting is specified.

Similar models have been discussed elsewhere (e.g. [45, 117, 121–123]). A unitary interaction  $U(\theta)$  is required as the first stage of the measurement, in order to specify the measurement setting, as in the selection of a polarizer angle  $\theta$  in a Bell-inequality experiment. The weak realism applies only to the system at the time  $t_0$  *after* a suitable unitary interaction has taken place to determine the setting [114]. The model has been shown consistent with Bell violations [117, 121].

The simulations and solutions of this paper are not inconsistent with the weak-realism model. The interpretation becomes that of macroscopic realism for a macroscopic superposition, and is linked with notion of "incompleteness of quantum mechanics" (Section IX.A). We see that while the  $x$  trajectories for  $\rho_{mix}$  and  $|\psi_{sup}\rangle$  are governed by identical equations, this does not conflict with the known discrepancy between superpositions and mixed states, since the  $p$  trajectories are different.

### C. Macroscopic-realism model

A third less restrictive model for realism builds from the weak-realism (wR) model in a way that naturally takes into account the measurement setting. We consider a macroscopic superposition

$$|\psi_m\rangle = (c_1|x_1\rangle + c_2|x_2\rangle)/\sqrt{2} \quad (8.1)$$

of two eigenstates of  $\hat{x}$ , where  $|x_1 - x_2| \gg 1$ . The outcome of  $\hat{x}$  is either  $x_1$  or  $x_2$ . The *macroscopic realism* (MR) model posits that the system in the state  $|\psi_m\rangle$  can be ascribed a definite value  $\lambda_M$  for the final outcome of the amplified measurement, which we call the pointer measurement [45, 117]. The value of  $\lambda_M$  is  $x_1$  or  $x_2$ . We call this a macroscopic realism (MR) model, after the definition given in [96]. The adoption of the MR model is consistent with the wR model, because the amplification of  $x$  (as opposed to  $p$ ) amounts to the specification of measurement setting.

The present definition applies to the state at time  $t_0$  prior to amplification (after the determination of the measurement setting), but makes *no* assumptions about the *nature* of the states corresponding to  $\lambda_M$ . The model is *macroscopically causal*, since the value of  $\lambda$  at time  $t_0$  determines the measurement outcome at the later time  $t_f$ , if the measurement takes place. There can be no change to  $\lambda$  due to a future measurement event. The solutions given in this paper support the MR model (refer Section IX.A).



#### D. Hybrid models: micro-retrocausal and macro-causal

The MR model implies for the macroscopic superposition that the outcome of the measurement  $\hat{x}$  is specified at time  $t_0$ . The causal relation is that the outcome at time  $t_f$  depends on the state at  $t_0$ .

In the simulations, the MR model goes hand-in-hand with the description of the trajectories at the microscopic level, which involves retrocausal *noise*. The sampling of the trajectories is consistent with the MR and wR models, since the sampling being based on the future boundary condition of the *mixture*  $\rho_{mix}$  of eigenstates. The trajectories for  $x$  that begin from the amplified value  $x_f \sim Gx_j$  at time  $t_f$  correspond to the initial Gaussian peak with a mean of  $x_j$ . The initial values  $Gx_1$  and  $Gx_2$  are *selected* with probabilities  $|c_1|^2$  and  $|c_2|^2$ , identically as for a system that at time  $t_0$  is in a statistical mixture  $\rho_{mix}$  of the two states  $|x_1\rangle$  and  $|x_2\rangle$ . This is because the interference terms in the  $Q$  function are not amplified. Yet, there is retrocausality in the simulations. The selection of the *precise* random noise value  $x_f - Gx_j$  is retrocausal because this value originates at the time  $t_f$  in the simulation. The constraint on the selection of this noise term that comes from the earlier time  $t_0$  is only that of the variance  $\sigma_x^2 = 1$  (in units where  $\hbar = 1$ ). There is retrocausality at the microscopic level of  $\hbar$ , but there is no retrocausality in the sense of a future measurement event or choice of setting affecting the present qubit value  $\lambda_M$  given for the system in the macroscopic superposition state (8.1) (at time  $t_0$ ).

#### E. Causal consistency and the meaning of retrocausality

This leads us to revisit the origin of the causal consistency which is inherent in the simulations, and to consider the ambiguity of the meaning of the retrocausality. The system evolved for a time  $t$  under the measurement interaction  $H_A$  is given by the state  $|\psi(t)\rangle = e^{-iH_A t/\hbar}|\psi_{sup}\rangle$ , equivalently given by the  $Q$  function  $Q(x, p, t)$ . The description  $|\psi(t)\rangle$  ( $Q(x, p, t)$ ) is *causal*: the function depends on  $t$ . We have proved the equivalence between the moments of  $Q(x, p, t)$  and those obtained by averaging over the trajectories  $x(t)$  and  $p(t)$  in Section IV.

It is counterintuitive that a system which is retrocausal, with trajectory values depending on boundary conditions at a future time  $t_f$ , can be consistent with the causal description, which is independent of  $t_f$ . The causal description, combined with the wR model, would imply that results of the measurement  $\hat{x}$  (say) at the time  $t$  cannot be affected by the choice of future time  $t_f$ . Hence, the solutions show there is no *actual* macroscopic retrocausality, in this sense.

The behavior is understood on noting that the noise  $\xi_1(t)$  that enters the retrocausal equations (7.4) at the

future boundary  $t_f$  has a fixed magnitude  $\sigma_{x/p}$  at the level of the vacuum, which does not depend on the measurement setting  $\theta$ , and is independent of the gain  $gt_f$ . The forward equations in the complementary variable are more complex, but these are causal equations. Similarly, the nature of the coupling of the trajectories for  $x$  and  $p$  is determined by the boundary condition in the present, at time  $t_0$ .

### IX. MACROSCOPIC REALISM: SCHRÖDINGER CAT, FRINGES AND THE MEASUREMENT PROBLEM

The causal model and realism models have been developed using an Occam's razor approach, looking for the simplest interpretation of the trajectories consistent with observations of causality at a macroscopic level. The argument for macroscopic realism can be made more strongly, based on Born's rule.

#### A. Macroscopic realism justified by trajectories

We consider the system prepared at time  $t = 0$  in the macroscopic superposition (8.1) of two eigenstates of  $\hat{x}$ , as depicted in of Figure 1 for  $x_2 = -x_1$ . The  $Q$  function  $Q_{sup}(x, p)$  for this state is given by (3.19) and is depicted as a probability density in Figure 1. The distribution is given in Figure 2.

Does this system satisfy macroscopic realism (MR)? For macroscopic superpositions, we see from the Figures that the separation  $\sim 2|x_1|$  between the peaks associated with the states  $|x_1\rangle$  and  $|-x_1\rangle$  is much greater than the peak variance  $\sigma_x^2(0) = 1$ . Hence, the trajectories stemming from a positive (negative)  $x$  in the future time  $t_f$  link directly back to a positive (negative)  $x$  in the present time  $t_0$ . There is a one-to-one correspondence between the initial and final regions e.g. the outcome  $x_1$  can connect only with values of  $x$  that are positive, at  $t = 0$ . For a given point  $x(t)$  on the trajectory, the inferred value for the outcome of  $\hat{x}$  is  $x(t)/G$ . This value becomes sharper as  $G \rightarrow \infty$ , approaching either  $x_1$  or  $-x_1$ , the relative error  $\delta/G$  due to the noise  $\delta$  becoming negligible.

Since for large enough amplification  $G$ , the trajectory value  $x(t)/G$  is the outcome of the measurement, *given by Born's rule*, we argue there is consistency with the macroscopic realism: The system at time  $t = 0$  is in a state that can be identified by the value of  $x(t)$  to give a definite result, either  $x_1$  or  $-x_1$ , for a future measurement of  $\hat{x}_1$ . The value is not sensitive to the hidden vacuum noise contribution  $\delta$  which depends on  $\xi(t)$ . One can assign a hidden variable  $\lambda_M$  to that system, where the value  $\lambda_M = 1$  implies the outcome  $x_1$  for  $\hat{x}$ , and the value  $\lambda_M = -1$  implies the outcome  $-x_1$  for  $\hat{x}$ .

We ask why this conclusion of macroscopic realism (MR) does not conflict with results demonstrating vio-

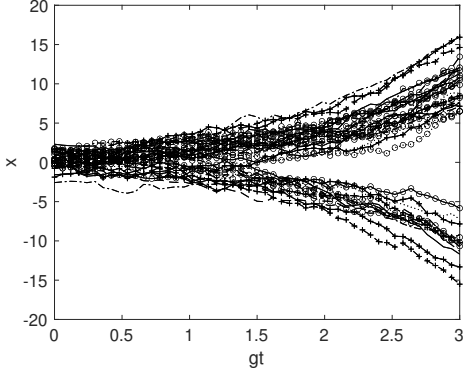


Figure 17. Measurement of  $\hat{x}$  and macroscopic realism: The system is prepared at time  $t = 0$  in a superposition  $|\psi_{sup}\rangle$  of eigenstates  $|x_1\rangle$  and  $|-x_1\rangle$  of  $\hat{x}$ . For large  $x_1$ , the outcomes for measurement  $\hat{x}$  that indicate the value of  $x_1$  (or  $-x_1$ ) allow the correct inference of an amplitude  $x$  corresponding to the state  $|x_1\rangle$  (or  $|-x_1\rangle$ ). On amplification, the system in a superposition  $|\psi_{sup}\rangle$  will evolve to a macroscopic superposition state (e.g. at the time  $gt_m = 2.5$ ). The simulations are consistent with macroscopic realism holding for the state at time  $t = t_m$ .

lations of macrorealism [96, 117, 124–126], or violations of macroscopic Bell inequalities [117, 127, 128], for similar macroscopic states. This can be explained by the extra assumptions involved in those inequalities, and to the dynamics of the measurement setting. The consistency of the trajectories with MR is for the measurement  $H_A$  of  $\hat{x}$ , which is direct *amplification*. The measurement setting has *already been established* at time  $t = 0$ . This is because, since we consider a macroscopic superposition, there has been amplification of  $\hat{x}$ . However, a measurement process involving a further change of measurement setting requires further unitary interactions, which occur over a time interval, and therefore produce a new final state, prior to an amplification process  $H_A$ . The tests that lead to violations of Leggett-Garg inequalities or of macroscopic Bell inequalities require changes of measurement setting. More details are given in [45, 117] and the companion paper [114].

### B. Schrödinger’s cat paradox: macroscopic realism and the incompleteness of quantum mechanics

The cat paradox seeks to understand the reality of the system in a macroscopic superposition [47, 111]. Such a state is prepared as part of the measurement process. Figure 17 shows this realization, in the model for measurement given by amplification  $H_A$ . The state formed at time  $t_m$  in the Figure is (taking  $r$  large)

$$e^{-iH_A t/\hbar}|\psi_{sup}\rangle = \frac{1}{\sqrt{2}}\{e^{-iH_A t/\hbar}|x_1\rangle + ie^{-iH_A t/\hbar}|-x_1\rangle\}. \quad (9.1)$$

For *sufficient amplification*  $G = e^{gt_m}$  after a time  $t_m$ , this state becomes a *macroscopic superposition* state, as also seen by the trajectories of Figures 1 and 17. The macroscopic realism model interprets the system in that state at the time  $t_m$  as satisfying macroscopic realism. This model allows the interpretation of macroscopic realism for the cat in the Schrödinger cat paradox [47], without consideration of decoherence. For the amplified state (9.1) at time  $t_m$ , the value for the measurement  $\hat{x}$  is determined by the variable  $\lambda_m$ , to be either  $x_1$  or  $-x_1$ . Macroscopic realism is satisfied by the definition of Leggett and Garg [96], because the system is in “one or other state” (defined by the amplitude) that will yield an outcome of either  $x_1$  or  $-x_1$ .

However, a simple analysis shows that these “states” with the real property  $\lambda_M$  cannot be *quantum* states. This is basically Schrödinger’s argument [47]. We follow the argument given in [45, 117, 129]. Let us examine the macroscopic superposition  $|\psi_{sup}\rangle$  given by (3.16) with  $x_1$  large. In the model, we assume this system satisfies macroscopic realism, and is in one of two “states” giving either  $x_1$  or  $-x_1$ . If these states are indeed quantum states, then this would imply the state  $|\psi_{sup}\rangle$  can be expressed as a probabilistic mixture

$$\rho_{mix}^Q = P_+\rho_+ + P_-\rho_-, \quad (9.2)$$

where  $\rho_{\pm}$  are quantum states giving an outcome  $\pm x_1$  for the measurement  $\hat{x}$ , and  $P_{\pm}$  are probabilities. However, the expression can be falsified for the predictions of the superposition state  $|\psi_{sup}\rangle$ . The uncertainty relation  $\Delta\hat{x}\Delta\hat{p} \geq 1$  holds for each  $\rho_{\pm}$ , and therefore for the mixture. Therefore, if the  $P_{\pm}(x)$  distributions associated with the positive and negative  $x_1$  are measured as Gaussians with variance  $\Delta\hat{x} \leq 1$  (as in Figure 9), it would be necessary that the distributions for  $P(p)$  satisfy  $\Delta\hat{p} \geq 1$ . However, the fringe distribution of Figure 12 gives  $\Delta\hat{p} < 1$ . The argument can be made that if macroscopic realism holds, then quantum mechanics is an incomplete description.

This apparent inconsistency between the completeness of (standard) quantum mechanics and macroscopic realism was demonstrated by the evaluation of the inferred states for  $x$  and  $p$ , *conditioned* on the outcome  $x_1$  or  $-x_1$ , in Section VI. The system described by these coupled sets of trajectories, at the time  $t_m$ , has a macroscopically determinate value of  $x$ , which is either positive or negative (as in Figure 17). However, the coupled trajectories for  $x$  and  $p$  do not correspond to quantum states, because the uncertainty product  $\Delta\hat{x}\Delta\hat{p}$  associated with the post-selected state reduces below 1.

### C. Interpretation of fringes

Fringes are observed in the conditional distribution  $P(p|x)$  for  $p$  evaluated at the boundary corresponding to time  $t = t_0 = 0$ . The conditional distribution is given by (6.1). We see from Figure 13 that these fringes do

not vanish if one considers the inferred distribution for  $p$  postselected on the outcome of  $\hat{x}$ . It is this feature that gives the reduced variance in  $\hat{p}$ , leading to the conclusion of incompleteness, that the post-selected state cannot be a quantum state.

The fringes would be expected to vanish, once it is known “which state the system was in”. This motivates a further calculation, in which the system is coupled to a separate meter, allowing a set-up where one may infer “which state the system is in” and simultaneously perform a measurement  $\hat{p}$  on the system  $A$ .

#### D. Measurement problem

The solutions of this paper show how macroscopic realism emerges with amplification. A system prepared in a superposition  $|\psi_{sup}\rangle$  of eigenstates  $|x_j\rangle$  can be considered to have a definite outcome  $x_j$  once the system has amplified sufficiently ( $G \rightarrow \infty$ ). This agrees with the measurement postulate that the outcome is an eigenvalue, and suggests that amplification plays an important part in the mechanism for the “collapse” of the wavefunction.

We also note that the inferred state conditioned on the outcome  $x_j$  (as calculated in Section VI) approaches the eigenstate  $|x_j\rangle$  for a macroscopic superposition. As the system is amplified, the superposition  $|\psi_{sup}\rangle$  evolves into a macroscopic superposition, which also agrees with the measurement postulate that the state after measurement is the eigenstate  $|x_j\rangle$ .

However, the amplification creating the macroscopic superposition state as in Figure 17 at the time  $t_m$  is *reversible*. One may return to the original state  $|\psi_{sup}\rangle$  at a time  $t_{2m}$  by attenuating  $x$ , applying the Hamiltonian  $H_A$  of (3.3) with  $g < 0$ . The complete process of the “collapse” to the eigenstate occurs when the process is *not* reversible. We expect this can be explained by the loss of information from the system when it is coupling to a second larger meter.

## X. CONCLUSION

We have presented a model (the objective field model, or  $Q$  model) for a quantum measurement involving trajectories of variables,  $x$  and  $p$ . We consider measurement of a quadrature phase amplitude ( $\hat{x}$  or  $\hat{p}$ ) on a single field mode, solving for the dynamics of a measurement interaction  $H_A$  which amplifies  $\hat{x}$  or  $\hat{p}$ . The model is based on the  $Q$  function  $Q(x, p)$ , which uniquely represents the quantum state, and on the equivalence of the dynamical equation for the  $Q$  function with forward-backward stochastic trajectories for amplitudes  $x$  and  $p$ . The model is derived within the framework of quantum field theory, is Lorenz invariant and can therefore be compatible with the standard model of particle physics. The equivalence is proved by two path-integral theorems. The forward and backward trajectories are linked according to the

conditional distribution provided by the  $Q$  function at the boundary corresponding to the time  $t_0 = 0$  of commencement of  $H_A$ . This leads to a non-acyclic causal feature. The measured variable ( $x$  or  $p$ ) is amplified, and requires a future boundary condition at time  $t_f$  (corresponding to the final time of interaction  $H_A$ ). While we have proved an equivalence between  $Q(x, p, t)$  and the trajectories for the forward-backward amplitudes for the measurement model, this is yet to be proved in general.

We have solved for the dynamical trajectories for several examples of initial states, confirming the equivalence to the  $Q$  function  $Q(x, p, t)$  throughout the dynamics, as verified through  $\chi^2$  statistical tests. Born’s rule is also verified in the limit of large amplification (when the measurement is complete). This provides independent verification of the theorems.

The description of the  $Q$ -model as “retrocausal” refers to the use of future boundary conditions for the backward trajectories. This can be misleading, since “retrocausal” is often understood to imply that an event from the future affects the outcome of a present event, in some way. In fact, the simulations of this paper give insight to show why this would *not* be the case. For the macroscopic superposition of Figure 1, in the hybrid causal model proposed, the outcome given by the eigenvalue  $\lambda_j \equiv x_j$  at time  $t_0$  is clearly not affected by the noise associated with the future boundary condition.

The theorems prove there is a causal consistency: The forward-backward trajectories at the time  $t$  provide equivalent moments to the quantum state given by  $Q(x, p, t)$  – which depends on the time of evolution  $t$ , *not* the future time  $t_f$ . Careful examination of the simulations shows why this is so. The input from the future boundary is vacuum noise. The set of outcomes  $x_j$  which are the eigenvalues are specified at the initial time, as the means  $x_j$  of weighted Gaussian “hills” in the  $Q$  function. The amplification that models the measurement can be described fully in terms of the *dynamical equation for the  $Q$  function*, as a generalised Fokker-Planck equation, and has the effect of amplifying the means  $x_j$  only, not the vacuum noise associated with the Gaussian hills. Similarly, the solutions show that the interference terms appearing in the  $Q$  function that distinguish a superposition of eigenstates  $|\psi_{sup}\rangle$  from a classical mixture  $\rho_{mix}$  of eigenstates are *not* amplified. Hence, the future boundary conditions for the mixed state and the superposition are identical. Procedurally, the simulation applies a future boundary condition as though the system were in a mixture  $\rho_{mix}$  i.e. equivalent to the assumption that the system is probabilistically at the initial time with outcome  $x_j$ . This motivates the causal models presented in Section VII. The superposition is distinguished from the mixture by the correlation between the  $x$  and  $p$  trajectories at the initial-time boundary i.e. by in the emergence of a causal loop. The  $p$  trajectories correspond to the complementary observable, and are not observed, dissipating to the vacuum level.

The solutions for the trajectories  $x(t)$  and  $p(t)$  of the  $Q$

model provide the possibility for a model of reality that appears *more complete* than given by standard quantum mechanics. This is shown for the superposition of two eigenstates of  $\hat{x}$ , by analyzing the connected sets of trajectories for  $x$  and  $p$ , and evaluating the variances associated with those distributions, postselected on the final outcome for the measurement of  $\hat{x}$ . The variance product reduces below that allowed by the Heisenberg uncertainty relation, implying that the trajectories associated with the definite outcome cannot be modeled by a quantum state  $|\psi\rangle$ . However, while this might provide a more complete *interpretation*, we emphasize that the solutions themselves arise *from* quantum mechanics. The solutions are not from a different theory.

Motivated by this, different models of realism have been presented, and analyzed for degree of consistency with the trajectories. This includes objective field realism (OFR) which proposes realism (similar to absorber theory) based on  $x$  and  $p$ ; weak realism (wR) which considers realism subject to the measurement setting; and macroscopic realism (MR). The analysis supports the validity of *macroscopic realism and macroscopic causality*, despite that retrocausality is embodied in the model. The conclusion is that the trajectories are consistent with macroscopic realism: A system prepared in a superposition of two macroscopically distinct eigenstates of  $\hat{x}$  at the time  $t_0$  has a well defined outcome  $\lambda_0$  for the result of the pointer measurement  $\hat{x}$ . However, there is microscopic noise (at the level of  $\hbar$ ) present in the final outcomes at the time  $t_f$ . This noise is present at all times, at the microscopic level, the values determined from both future and past boundary conditions. The conclusion is consistent with macroscopic causality, since the well-defined outcome  $\lambda_0$  is defined at the time  $t_0$ , independent of any future event, giving the outcome of the measurement  $\hat{x}$  if that measurement were to be performed (without a change of measurement setting).

A macroscopic-realism model provides an interpretation of the Schrödinger cat paradox. Macroscopic real-

ism holds for the macroscopic superposition state, but the associated “states” of the system at the microscopic level cannot be described completely by standard quantum mechanics. The macroscopic-realism model does not conflict with the known violations of macrorealism and of macroscopic local realism (as shown through violations of Leggett-Garg [96] and macroscopic Bell inequalities [117, 127, 128]). In those set-ups, there are changes of measurement settings and hence extra assumptions are involved. Another more restrictive model for realism that is not inconsistent with the trajectories of the  $Q$  model is the weak-realism (wR) (refer also to [117, 121, 128]). The wR model requires further analysis accounting for the dynamics of the interactions associated with a change of measurement setting.

A natural question is whether or how the  $Q$ -model explains Einstein-Podolsky-Rosen entanglement and Bell nonlocality. Einstein-Podolsky-Rosen (EPR) correlations are realised for the quadrature phase amplitudes  $\hat{x}$  and  $\hat{p}$  of a system prepared in a two-mode squeezed state [130, 131]. Hence, the measurements can be modelled by the amplification  $H_A$  studied in this paper. Similarly, Bell nonlocality can be detected for quadrature phase amplitude measurements, provided suitable changes of measurement settings can be realised, for example, as phase shifts [132–135]. EPR argued that quantum mechanics was incomplete, based on the premise of local realism. Local realistic theories are falsified by Bell nonlocality. In the companion paper [114], we show how the forward-backward equations of the  $Q$  model can be used to simulate EPR and Bell correlations.

## ACKNOWLEDGMENTS

This work was funded through Australian Research Council Discovery Project Grants DP180102470 and DP190101480. We thank NTT Research for technical help and motivation for this project.

- 
- [1] N. Bohr, *Essays 1958-1962 on Atomic Phys. and Human Knowledge*, Bohr, Niels: Philosophical writings, Vol. 3 (Ox Bow Press, Woodbridge, USA, 1987).
  - [2] X.-s. Ma, J. Kofler, and A. Zeilinger, *Rev. Mod. Phys.* **88**, 015005 (2016).
  - [3] J. A. Wheeler, in *Mathematical foundations of quantum theory* (Elsevier, 1978) pp. 9–48.
  - [4] J. A. Wheeler and W. H. Zurek, *Quantum theory and measurement*, Vol. 40 (Princeton University Press, 2014).
  - [5] P. A. M. Dirac, *Rev. Mod. Phys.* **17**, 195 (1945).
  - [6] J. A. Wheeler and R. P. Feynman, *Rev. Mod. Phys.* **17**, 157 (1945).
  - [7] J. A. Wheeler and R. P. Feynman, *Rev. Mod. Phys.* **21**, 425 (1949).
  - [8] J. S. Bell, *Phys.* **1**, 195 (1964).
  - [9] N. Brunner, D. Cavalcanti, S. Pironio, V. Scarani, and S. Wehner, *Rev. Mod. Phys.* **86**, 419 (2014).
  - [10] J. F. Clauser and A. Shimony, *Rep. Prog. Phys.* **41**, 1881 (1978).
  - [11] D. Pegg, *Phys. Lett. A* **78**, 233 (1980).
  - [12] J. G. Cramer, *Phys. Rev. D* **22**, 362 (1980).
  - [13] D. T. Pegg, *Physica Scripta* **1986**, 14 (1986).
  - [14] J. G. Cramer, *Rev. Mod. Phys.* **58**, 647 (1986).
  - [15] P. H. Eberhard and R. R. Ross, *Foundations of Phys. Lett.* **2**, 127 (1989).
  - [16] Y. Aharonov, P. G. Bergmann, and J. L. Lebowitz, *Phys. Rev.* **134**, B1410 (1964).
  - [17] M. O. Scully and K. Drühl, *Phys. Rev. A* **25**, 2208 (1982).
  - [18] M. O. Scully, B.-G. Englert, and H. Walther, *Nature* **351**, 111 (1991).
  - [19] U. Mohrhoff, *Am. J. Phys.* **64**, 1468 (1996).
  - [20] B.-G. Englert, M. O. Scully, and H. Walther, *Am. J.*

- Phys. **67**, 325 (1999).
- [21] Y.-H. Kim, R. Yu, S. P. Kulik, Y. Shih, and M. O. Scully, Phys. Rev. Lett. **84**, 1 (2000).
  - [22] S. P. Walborn, M. O. T. Cunha, S. Pádua, and C. H. Monken, Phys. Rev. A **65**, 033818 (2002).
  - [23] V. Jacques, E. Wu, F. Grosshans, F. Treussart, P. Grangier, A. Aspect, and J.-F. Roch, Science **315**, 966 (2007).
  - [24] H. Price, Studies in History and Philosophy of Science Part B: Studies in History and Philosophy of Modern Phys. **39**, 752 (2008).
  - [25] Y. Aharonov and L. Vaidman, Time in quantum mechanics, 399 (2008).
  - [26] R. Ionicioiu and D. R. Terno, Phys. Rev. Lett. **107**, 230406 (2011).
  - [27] J.-S. Tang, Y.-L. Li, X.-Y. Xu, G.-Y. Xiang, C.-F. Li, and G.-C. Guo, Nature Photonics **6**, 600 (2012).
  - [28] A. Peruzzo, P. Shadbolt, N. Brunner, S. Popescu, and J. L. O'Brien, Science **338**, 634 (2012).
  - [29] F. Kaiser, T. Coudreau, P. Milman, D. B. Ostrowsky, and S. Tanzilli, Science **338**, 637 (2012).
  - [30] X.-S. Ma, J. Kofler, A. Qarry, N. Tetik, T. Scheidl, R. Ursin, S. Ramelow, T. Herbst, L. Ratschbacher, A. Fedrizzi, *et al.*, Proceedings of the National Academy of Sciences **110**, 1221 (2013).
  - [31] R. Ionicioiu, T. Jennewein, R. B. Mann, and D. R. Terno, Nature Communications **5**, 1 (2014).
  - [32] A. G. Manning, R. I. Khakimov, R. G. Dall, and A. G. Truscott, Nature Phys. **11**, 539 (2015).
  - [33] S.-B. Zheng, Y.-P. Zhong, K. Xu, Q.-J. Wang, H. Wang, L.-T. Shen, C.-P. Yang, J. M. Martinis, A. N. Cleland, and S.-Y. Han, Phys. Rev. Lett. **115**, 260403 (2015).
  - [34] R. Chaves, G. B. Lemos, and J. Pienaar, Phys. Rev. Lett. **120**, 190401 (2018).
  - [35] R. Rossi Jr, Phys. Rev. A **96**, 012106 (2017).
  - [36] A. S. Rab, E. Polino, Z.-X. Man, N. Ba An, Y.-J. Xia, N. Spagnolo, R. Lo Franco, and F. Sciarrino, Nature Communications **8**, 1 (2017).
  - [37] W. Qin, A. Miranowicz, G. Long, J. Q. You, and F. Nori, npj Quantum Information **5**, 1 (2019).
  - [38] E. Polino, I. Agresti, D. Poderini, G. Carvacho, G. Milani, G. B. Lemos, R. Chaves, and F. Sciarrino, Phys. Rev. A **100**, 022111 (2019).
  - [39] R. Kastner, Foundations of Phys. **49**, 717 (2019).
  - [40] H.-L. Huang, Y.-H. Luo, B. Bai, Y.-H. Deng, H. Wang, Q. Zhao, H.-S. Zhong, Y.-Q. Nie, W.-H. Jiang, X.-L. Wang, *et al.*, Phys. Rev. A **100**, 012114 (2019).
  - [41] S. Yu, Y.-N. Sun, W. Liu, Z.-D. Liu, Z.-J. Ke, Y.-T. Wang, J.-S. Tang, C.-F. Li, and G.-C. Guo, Phys. Rev. A **100**, 012115 (2019).
  - [42] K. B. Wharton and N. Argaman, Rev. Mod. Phys. **92**, 021002 (2020).
  - [43] P. D. Drummond, Phys. Rev. Research **3**, 013240 (2021).
  - [44] B. R. La Cour and T. W. Yudichak, Phys. Rev. A **103**, 062213 (2021).
  - [45] M. Thenabadu and M. D. Reid, Phys. Rev. A **105**, 062209 (2022).
  - [46] T. J. Herzog, P. G. Kwiat, H. Weinfurter, and A. Zeilinger, Phys. Rev. Lett. **75**, 3034 (1995).
  - [47] E. Schrödinger, Naturwissenschaften **23**, 823 (1935).
  - [48] D. Bohm, Phys. Rev. **85**, 166 (1952).
  - [49] H. Everett, Rev. Mod. Phys. **29**, 454 (1957).
  - [50] P. Pearle, Phys. Rev. D **13**, 857 (1976).
  - [51] A. Bassi, K. Lochan, S. Satin, T. P. Singh, and H. Ulbricht, Rev. Mod. Phys. **85**, 471 (2013).
  - [52] M. J. W. Hall, D.-A. Deckert, and H. M. Wiseman, Phys. Rev. X **4**, 041013 (2014).
  - [53] P. D. Drummond and M. D. Reid, Phys. Rev. Research **2**, 033266 (2020).
  - [54] M. Born, Science **122**, 675 (1955).
  - [55] J. Bell, Phys. world **3**, 33 (1990).
  - [56] O. Oreshkov, F. Costa, and Č. Brukner, Nature Communications **3**, 1 (2012).
  - [57] R. Chaves and T. Fritz, Phys. Rev. A **85**, 032113 (2012).
  - [58] C. J. Wood and R. W. Spekkens, New J. Phys. **17**, 033002 (2015).
  - [59] E. G. Cavalcanti, Phys. Rev. X **8**, 021018 (2018).
  - [60] J. Pearl and E. Cavalcanti, Quantum **5**, 518 (2021).
  - [61] F. Costa and S. Shrapnel, New J. Phys. **18**, 063032 (2016).
  - [62] J.-M. A. Allen, J. Barrett, D. C. Horsman, C. M. Lee, and R. W. Spekkens, Phys. Rev. X **7**, 031021 (2017).
  - [63] S. Shrapnel, The British Journal for the Philosophy of Science **70**, 1 (2019).
  - [64] J. Barrett, R. Lorenz, and O. Oreshkov, Nature Communications **12**, 1 (2021).
  - [65] J. Pienaar, Phys. Rev. A **101**, 012104 (2020).
  - [66] J.-M. A. Allen, J. Barrett, D. C. Horsman, C. M. Lee, and R. W. Spekkens, Phys. Rev. X **7**, 031021 (2017).
  - [67] M. Weilenmann and R. Colbeck, Quantum **4**, 236 (2020).
  - [68] G. Chiribella, Phys. Rev. A **86**, 040301(R) (2012).
  - [69] F. A. Pollock, C. Rodríguez-Rosario, T. Frauenheim, M. Paternostro, and K. Modi, Phys. Rev. Lett. **120**, 040405 (2018).
  - [70] M. Araújo, F. Costa, and Č. Brukner, Phys. Rev. Lett. **113**, 250402 (2014).
  - [71] M. Araújo, C. Branciard, F. Costa, A. Feix, C. Giarmatzi, and Č. Brukner, New J. Phys. **17**, 102001 (2015).
  - [72] O. Oreshkov and C. Giarmatzi, New J. Phys. **18**, 093020 (2016).
  - [73] C. Giarmatzi, in *Rethinking Causality in Quantum Mechanics* (Springer, 2019) pp. 125–150.
  - [74] M. Gachechiladze, N. Miklin, and R. Chaves, Phys. Rev. Lett. **125**, 230401 (2020).
  - [75] P. J. Daley, K. J. Resch, and R. W. Spekkens, Phys. Rev. A **105**, 042220 (2022).
  - [76] M. Araújo, P. A. Guérin, and Ä. Baumeler, Physical Review A **96**, 052315 (2017).
  - [77] G. Chiribella, G. M. D'Ariano, P. Perinotti, and B. Valiron, Physical Review A **88**, 022318 (2013).
  - [78] V. Vilasini and R. Colbeck, Physical Review A **106**, 032204 (2022).
  - [79] P. Blasiak and E. Borsuk, Physical Review A **105**, 012207 (2022).
  - [80] V. Gebhart, L. Pezzè, and A. Smerzi, Physical Review Letters **127**, 140401 (2021).
  - [81] T. A. Brun, Foundations of Physics Letters **16**, 245 (2003).
  - [82] S. Aaronson and J. Watrous, Proceedings of the Royal Society A: Mathematical, Physical and Engineering Sciences **465**, 631 (2009).
  - [83] T. A. Brun, J. Harrington, and M. M. Wilde, Physical Review Letters **102**, 210402 (2009).
  - [84] M. J. W. Hall and C. Branciard, Physical Review A **102**, 052228 (2020).
  - [85] W. Struyve, Rep. Prog. Phys. **73**, 106001 (2010).

- [86] B. F. Toner and D. Bacon, Phys. Rev. Lett. **91**, 187904 (2003).
- [87] V. Scarani, J.-D. Bancal, A. Suarez, and N. Gisin, Foundations of Phys. **44**, 523 (2014).
- [88] S. Hossenfelder and T. Palmer, Frontiers in Phys. **8**, 139 (2020).
- [89] V. Vilasini and R. Colbeck, Physical Review Letters **129**, 110401 (2022).
- [90] G. Castagnoli, Phys. Rev. A **104**, 032203 (2021).
- [91] G. Castagnoli, Foundations of Physics **48**, 333 (2018).
- [92] G. Castagnoli, E. Cohen, A. Ekert, and A. Elitzur, Foundations of Physics **49**, 1200 (2019).
- [93] P. D. Drummond and M. D. Reid, Entropy **23**, 749 (2021).
- [94] S. Friederich, The British Journal for the Philosophy of Science **0**, null (2021), <https://doi.org/10.1086/716196>.
- [95] R. W. Spekkens, Phys. Rev. A **75**, 032110 (2007).
- [96] A. J. Leggett and A. Garg, Phys. Rev. Lett. **54**, 857 (1985).
- [97] D. Deutsch, Physical Review D **44**, 3197 (1991).
- [98] K. Husimi, Proc. Physical Math. Soc. Jpn. **22**, 264 (1940).
- [99] H. P. Yuen, Phys. Rev. A **13**, 2226 (1976).
- [100] R. R. Joseph, L. E. Rosales-Zárate, and P. D. Drummond, J. Phys. A **51**, 245302 (2018).
- [101] L. E. C. Rosales-Zárate and P. D. Drummond, New J. Phys. **17**, 032002 (2015).
- [102] B. Yurke and D. Stoler, Phys. Rev. Lett. **57**, 13 (1986).
- [103] P. D. Drummond and M. Hillery, *The quantum theory of nonlinear optics* (Cambridge University Press, 2014).
- [104] R. R. Joseph, P. D. Drummond, and L. E. C. Rosales-Zárate, Phys. Rev. A **104**, 062208 (2021).
- [105] R. Stratonovich, SIAM J. Control **4**, 362 (1966).
- [106] R. Graham, Zeitschrift für Physik B **26**, 281 (1977).
- [107] K. Pearson, The London, Edinburgh, and Dublin Philosophical Magazine and Journal of Science **50**, 157 (1900).
- [108] P. D. Drummond, B. Opanchuk, A. Dellios, and M. D. Reid, Phys. Rev. A **105**, 012427 (2022).
- [109] P. D. Drummond and I. K. Mortimer, J. Comput. Phys. **93**, 144 (1991).
- [110] A. L. Rukhin, J. Soto, J. R. Nechvatal, M. E. Smid, E. B. Barker, S. D. Leigh, M. Levenson, M. Vangel, D. L. Banks, *et al.*, *A statistical test suite for random and pseudorandom number generators for cryptographic applications*, Tech. Rep. (2010).
- [111] F. Fröwis, P. Sekatski, W. Dür, N. Gisin, and N. Sangouard, Rev. Mod. Phys. **90**, 025004 (2018).
- [112] M. D. Reid, J. Phys. A. **50**, 41LT01 (2017).
- [113] E. Cavalcanti and M. D. Reid, Phys. Rev. A **77**, 062108 (2008).
- [114] M. D. Reid and P. D. Drummond (2023).
- [115] P. A. M. Dirac, Proc. R. Soc. London. A **167**, 148 (1938).
- [116] L. Wittgenstein, *Tractatus Logico-Philosophicus* (Harcourt, Brace and Company, New York, 1922).
- [117] M. Thenabadu and M. D. Reid, Phys. Rev. A **105**, 052207 (2022).
- [118] J. S. Bell, *Speakable and unspeakable in quantum mechanics: Collected papers on quantum philosophy* (Cambridge University Press, 2004).
- [119] S. Kochen and E. P. Specker, in *The logico-algebraic approach to quantum mechanics* (Springer, 1975) pp. 293–328.
- [120] S. Kochen and E. P. Specker, Journal of Mathematics and Mechanics **17**, 59 (1967).
- [121] P. Grangier, Entropy **23**, 1660 (2021).
- [122] A. Auffèves and P. Grangier, International Journal of Quantum Information **14**, 1640002 (2016).
- [123] A. Auffèves and P. Grangier, Foundations of Phys. **46**, 121 (2016).
- [124] C. Emary, N. Lambert, and F. Nori, Rep. Prog. Phys. **77**, 016001 (2013).
- [125] G. C. Knee, K. Kakuyanagi, M.-C. Yeh, Y. Matsuzaki, H. Toida, H. Yamaguchi, S. Saito, A. J. Leggett, and W. J. Munro, Nature Communications **7**, 1 (2016).
- [126] H.-Y. Ku, N. Lambert, F.-J. Chan, C. Emary, Y.-N. Chen, and F. Nori, npj Quantum Information **6**, 98 (2020).
- [127] H. Jeong, M. Paternostro, and T. C. Ralph, Phys. Rev. Lett. **102**, 060403 (2009).
- [128] M. Thenabadu, G.-L. Cheng, T. L. H. Pham, L. V. Drummond, L. Rosales-Zárate, and M. D. Reid, Phys. Rev. A **102**, 022202 (2020).
- [129] M. D. Reid, Phys. Rev. A **100**, 052118 (2019).
- [130] M. D. Reid, Phys. Rev. A **40**, 913 (1989).
- [131] M. D. Reid, P. D. Drummond, W. P. Bowen, E. G. Cavalcanti, P. K. Lam, H. A. Bachor, U. L. Andersen, and G. Leuchs, Rev. Mod. Phys. **81**, 1727 (2009).
- [132] U. Leonhardt and J. A. Vaccaro, *Journal of Modern Optics*, Journal of Modern Optics **42**, 939 (1995).
- [133] A. Gilchrist, P. Deuar, and M. D. Reid, Phys. Rev. Lett. **80**, 3169 (1998).
- [134] A. Gilchrist, P. Deuar, and M. D. Reid, Phys. Rev. A **60**, 4259 (1999).
- [135] K. Banaszek and K. Wódkiewicz, Phys. Rev. Lett. **82**, 2009 (1999).